A Realistic Numerical Model of a Muffin Fan for Thermal Management of Electronic Equipment

A THESIS
SUBMITTED TO THE FACULTY OF
UNIVERSITY OF MINNESOTA
BY

Grant S. Backes

IN PARTIAL FULFILLMENT OF THE REQUIREMENTS
FOR THE DEGREE OF
MASTER OF SCIENCE

Ephraim M. Sparrow

March of 2014

Acknowledgements

A special thanks to my advisors Eph Sparrow and John Gorman for all of their hard work and dedication.

Abstract

The proper functioning of electronic equipment requires that temperatures not exceed specified upper bounds. To fulfill this limitation, small axial fans (called muffin fans) are commonly used. The fans move air by their curved rotating blades. The rotation of the blades imparts swirl to the air.

In the published literature, the coolant airflow entering the electronic-equipment housing is assumed arbitrarily prescribable. The present investigation is based on a realistic model both of the rotating nature of the airflow and of the geometry of the thermal management system. The thermal management system consists of an extensive array of pin fins which receive heat from the electronic equipment.

The research was implemented by means of numerical simulation. The results encompass heat transfer rates and patterns of fluid flow. Of interest is the degree of non-uniformity of the heat transferred by individual fins as a function of their location in the array.

Table of Contents

List of Tables

List of Figures

INTRODUCTION

As electronic devices continue to shrink in size and power demands increase, the heat generated per unit volume has dramatically increased. When these devices attain temperatures that exceed a threshold value, performance decreases and the device may even malfunction. Accordingly, the importance of thermal management is of interest. Many methods of heat extraction are available. A system of fins and an air-moving fan, as shown in Figure 1, is often utilized in compact devices to remove heat. Heat sinks typically consist of an array of either straight, curved, or pin fins made from a highly conductive material, such as aluminum, with the primary goal of increasing surface area over which a coolant fluid can flow.

Ideally, the heat sink base is in intimate thermal contact with the electronic device so that heat conduction can function with high effectiveness. Thermal energy is dissipated from the heat sink primarily by means of forced air convection, driven by a small fan. In general, the rate of heat extraction is increased with more surface area and higher airflow rates. As the surface area of the heat sink is increased (e.g., increase of fin height, number of fins, fin thickness, etc.), it is likely that the fan must overcome a higher pressure drop. Since space in a compact device is limited and cost of materials is a critical issue, overdesigning the fins is not cost effective. Thus, there is a delicate interplay between maximizing heat transfer and minimizing the pressure drop the fan must overcome.

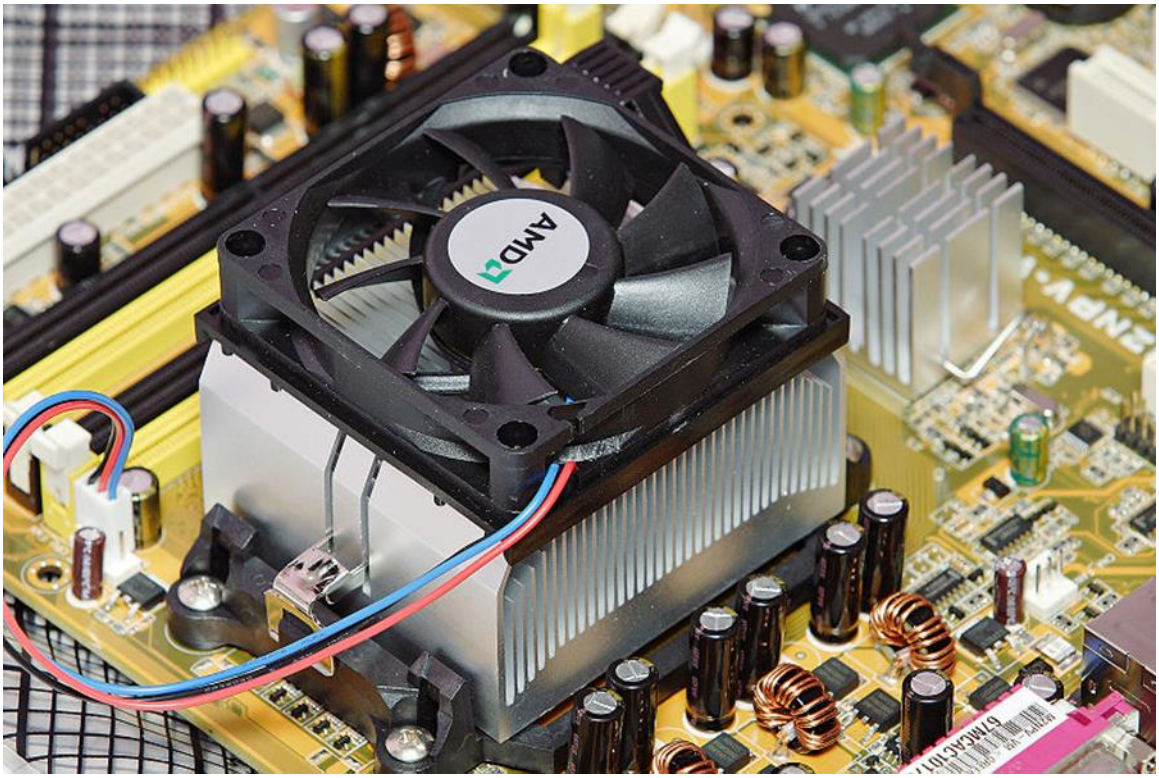

Figure 1: Straight fin array and fan assembly in a compact electronic device.

LITERATURE REVIEW

A literature review has been performed on heat transfer and fluid mechanics involving a fin array and air passing through the array. In the universe of fin types, pin fins appear to have emerged as preferred for compact thermal management tasks. A representative pin fin array is pictured in Figure 2. As seen there, each individual fin is a circular cylinder, one end of which is mated with a square plate. Although circular-cylinder pin fins are commonly encountered, other shapes are also used in practice.

The present investigation of pin fin arrays is implemented by numerical simulation. In this light, the primary focus of the literature review is to establish the current state of knowledge that has been developed from prior applications of this methodology. Agonafer and Free [1] numerically investigated the heat transfer performance of arrays of both circular and square pin fins. The flow was delivered to the arrays in the direction parallel to the axes of the fins and was oriented so that the air entered from the fin-tip end of the array.

Figure 2: Representative pin fin array.

A second flow configuration was such that the coolant air passed in crossflow over the fins. Both laminar and turbulent flows were considered. Although the airflow provided by an actual fan was not modeled, the swirl that is inherent in axial-fan-delivered flow was represented by a tangential component superimposed on a uniform inlet velocity profile. For flow entering the array parallel to the pin fin axes, it was found

that the best heat transfer performance occurred for those fins which were situated directly downstream of the fan blades, while poor performance was noted for fins positioned downstream of the hub of the envisioned fan. In view of the complexity of the fluid flow field, it is noteworthy that the simulations were performed with only 16,000 nodes. This minimal nodal count suggests a possible accuracy issue.

Behnia et al. [2] numerically investigated the performance of both staggered and inline pin fin arrays over which air passed in crossflow. The pin fin cross sections included square, circular, and elliptical. Major assumptions included the absence of a fan, a uniform inlet velocity, and laminar flow. Among these, the uniformity of the incoming flow and the absence of swirl represent major departures from reality. It was found that, for all of the investigated pin fin shapes, the staggered array gave superior performance. Jet-impinging, axially oriented flow delivered to an array of square pin fins was explored both numerically and experimentally by Maveety et al. [3]. For the simulation, experimentally determined inlet velocities were used along with a turbulence model and time dependence. It was found that both increasing Reynolds number and fin height results in a lower thermal resistance. Numerical results were found to be in good agreement with experimental results for medium-high Re numbers.

A highly simplified analytical model was used by Kobus and Oshio [4] which required values of the heat transfer coefficient for its implementation. Experiments were performed to determine the needed coefficient values. Shah et al. [5] numerically simulated axially delivered flow to 17 different pin geometries. The goal of this study was to investigate the effect of fin position in the array on heat transfer. Particular focus

was given to fins at the center of the array. Multiple incoming flow conditions, determined via wind tunnel experiments, were considered along with a turbulent flow model. It was found that removing material from the center of the heat sink results in better heat transfer.

Zheng and Wirtz [6] experimentally found friction factor and heat transfer correlation equations for impinging flow on circular pin fins. Parameters included are coolant flow rate, fin density, and fin height. Jet-driven impingement flow was also studied and compared to fan-driven flow. It was found that for a given pin fin array and flow rate, fan-driven flow yields better heat transfer. Jonsson and Moshfegh [7] experimentally analyzed parallel flow over 42 different pin and straight fin geometries. Correlations for heat transfer and pressure drop resulted. Correlations are dependent upon duct height, duct width, fin height, fin thickness, and fin-to-fin distance.

Numerical simulation and optimization of impinging flow onto pin fins was carried out by Park et al [8]. Pin fin parameters considered are height, width, and fin-to-fan distance. The constant downward velocity is assumed, along with an angular component. Flow is also assumed to be steady and the standard K-Epsilon model is used for turbulence. The effects of natural convection are considered. Curves of pressure drop and thermal resistance vs. fin height, width, and fin-to-fan distance are given. A mathematical model for optimization is presented and results discussed.

Impinging flow onto streamlined fins is numerically investigated by Jian-Hui and Chun-Xin [9]. Unlike much of the previous literature, they explicitly simulate the fan, rather than assume or use experimental data to determine incoming velocity. The flow is

assumed to be steady and the RNG K-Epsilon model is used. Streamlined fins are compared to traditional straight fins and are found to be better at transferring heat. They also study the rate of entropy generation.

Huang, Lu, and Ay [10] numerically simulated impinging flow onto pin fins. Similar to Jian-Hui and Chun-Xin [9], the fan is explicitly simulated. This study assumed steady state and used the standard K-Epsilon model of turbulence. Three different heat sinks were considered, with the goal of minimizing the maximum temperature of the heat sink. It was found that increased fin height and decreased fin thickness is optimum.

NUMERICAL SIMULATION

Physical Model

As was noted in the foregoing, the modeled physical situations were solved by means of numerical simulation. A total of five cases are investigated here. These include: (1) a baseline case of fan-driven impinging flow on 15 mm long cylindrical pin fins, with an adiabatic heat sink base, (2) same as the baseline case except that the heat sink base is at a constant dimensionless temperature equal to one (same temperature as that of the pin fins), (3) same as the baseline case except that the fin length has been increased from 15 to 25 mm, (4) same as the baseline case except that a shroud has been inserted on the housing of the fan, and (5) same as the baseline case except that the fan has been physically reversed in direction. Only the baseline case will be discussed in

detail, since the other cases have nearly identical geometry, mesh, and boundary conditions.

A quadrant section of the pin fin array and its attendant fan are displayed in Figure 3. The fan proper has eight blades, thereby enabling the existence of quadrant symmetry. The use of the quadrant section was motivated to diminish the execution time of the numerical solutions. A unique feature of the present investigation is that fan rotation is an integral part of the solution strategy. In most of the prior literature, the fluid entering the fin array was prescribed and not created by an actual fan.

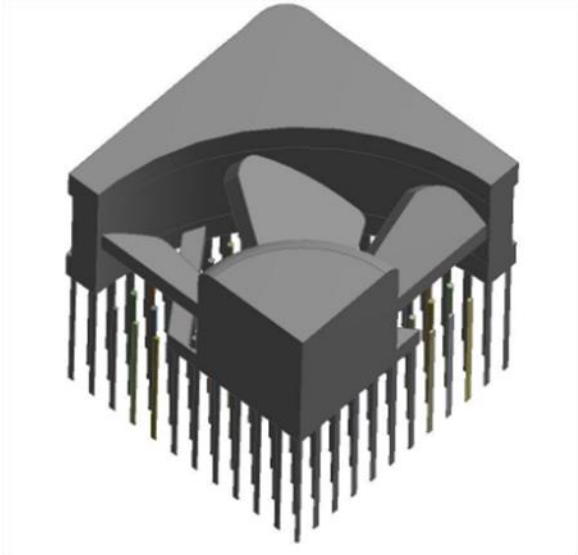

Figure 3: Quadrant section of the pin fin array and the attendant fan.

The air is drawn from above and enters the fan through the annular space between the frame and the hub. The frame is a stationary structure while hub and blades rotate. The air exits the fan through the annular space. The exiting flow is three-dimensional and contains a strong swirl component. With a 12-volt input, the fan operates at 5600

rpm. The CAD drawing which served as the baseline for Figure 3 is available online via http://www.sofasco.com/dcaxial.html.

In addition to the geometry shown in Figure 3, the specification of the solution domain is another significant geometrical feature. A plan view of the solution domian is displayed in Figure 4 and an elevation view is conveyed in Figure 5. The light-dashed rectangle in Figure 5 represents an optional shroud whose function is to guard against short-circuiting of air discharged from the fin array from being drawn into the inlet of the fan.

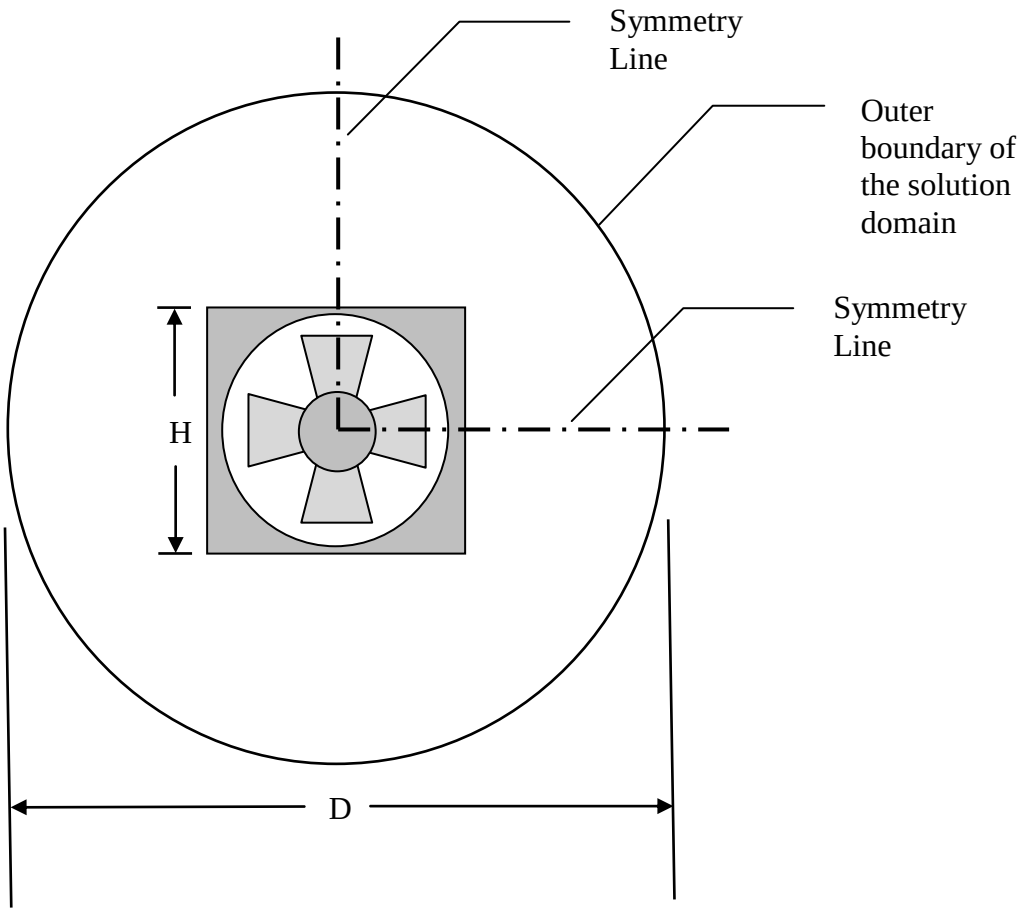

Figure 4: Plan view of the solution domain with the fan in place.

Aside from the fan, fin array, and optional shroud, the remainder of the solution domain is occupied by moving air. The dimensions of all of the components of the problem are found in Table 1.

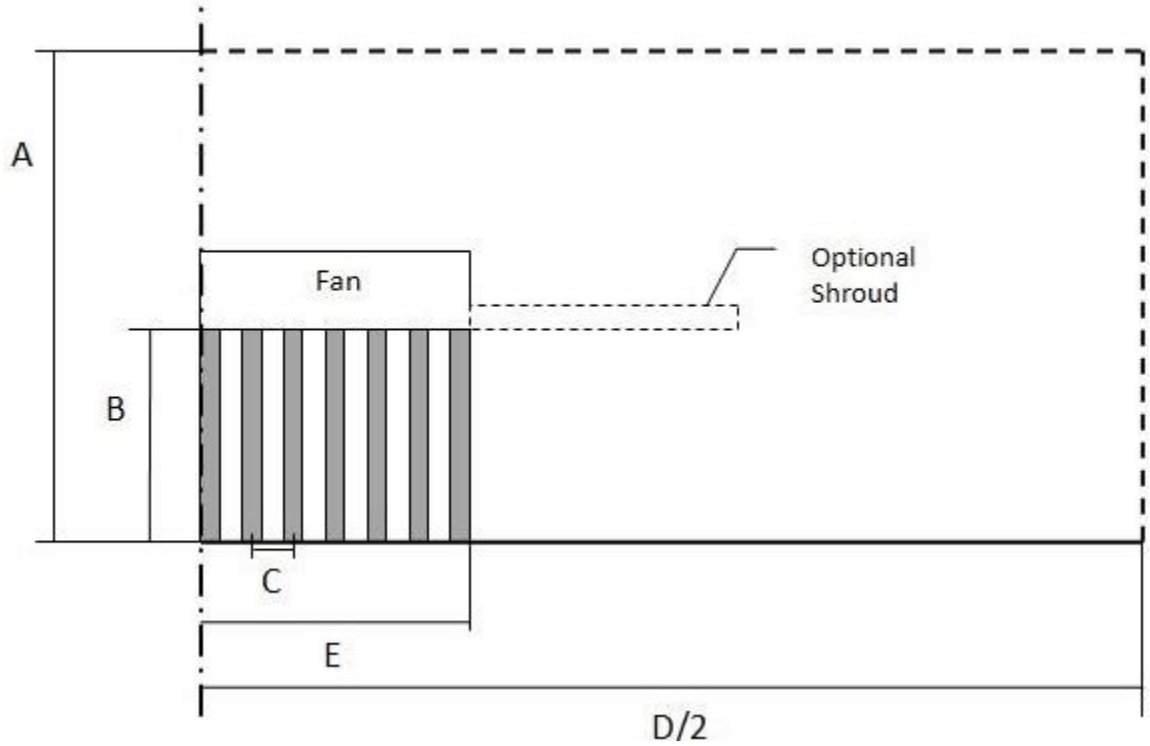

Figure 5: Elevation view of the solution domain.

Table 1: Dimensions of all of the components of the problem. Additional values are listed for Case (3), in which the domain increases in size due to elongated fins.

Pin Fin Array	
Number of fins in array	529
Fin height (length B in Figure 5)	15, 25 mm
Fin diameter	0.5 mm
Pitch (length C in Figure 5)	2.2 mm
Array Size (Length E in Figure 5)	50x50 mm
Fan	
Hub diameter	22 mm
Outer diameter of flow annulus	43.6 mm
Face	50x50 mm

Depth	15 mm
Optional Shroud	
Shroud thickness	1 mm
Shroud inner square lengths	50x50 mm
Shroud outer circle diameter	100 mm
Solution Domain (Cylindrical)	
Height (Length A in Figure 5)	100, 110 mm
Diameter (Length D in Figures 4 and 5)	300 mm

Numerical Model

The fluid flow problem in question is three-dimensional, unsteady, and turbulent. The partial differential equations describing the flow will be displayed later. It is well established that even with the maximum available computer power, the partial differential equations cannot be solved exactly. Rather, they must be discretized and transformed into algebraic equations. The process of discretization converts the mass continuum which occupies the solution domain into an array of discrete volume elements. Each element hosts discrete points called nodes. The actual numerical solutions are performed at the nodes. When discretized, the solution domain is said to be meshed.

The discretized solution domain can be seen in Figure 6. The large, central image displays the entire domain. Select regions within the dashed boxes are shown in more detail. A total of 5.7 million nodes are used in Case (1), as seen in Table 2. Table 3 shows the number of nodes used in other cases. A similar number of nodes are used in the other cases. It can be seen that the mesh is finer near solid surfaces such as the fan and the pin fins, as is appropriate due to the velocity and temperature gradients in those regions. A mesh independence study was performed for the baseline case with an original mesh consisting of 5.7 million nodes and a second mesh composed of 10.4

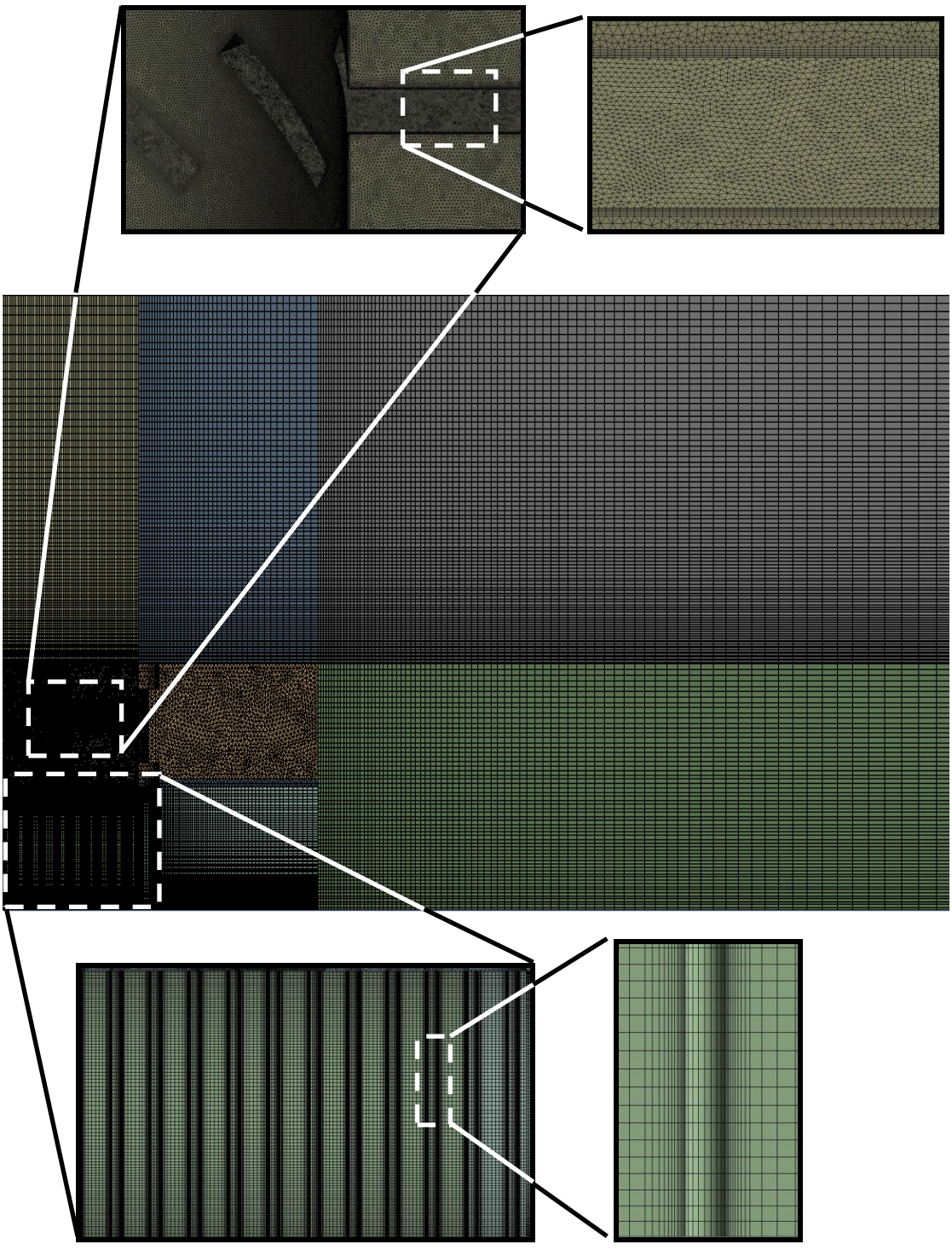

Figure 6: Discretized solution domain of Case (1). Enlarged images of the regions within the dashed boxes are presented.

million nodes. It was found that the heat transfer results for the respective meshes differed by 0.27%, seen in Table 2 and Figure 7.

Table 2: Results for the mesh independence test for Case (1).

Case (1)	**Number of nodes (millions)**	**Time averaged heat transfer (Watts)**
Original Mesh	5.7	1.130
Refined Mesh	10.4	1.127

Table 3: Number of nodes for each case simulated.

Case	**Number of nodes (millions)**
Case (2): Base temperature equal to one	5.7
Case (3): 25 mm fins	5.6
Case (4): Shrouded	6.0
Case (5): Reversed Fan	5.5

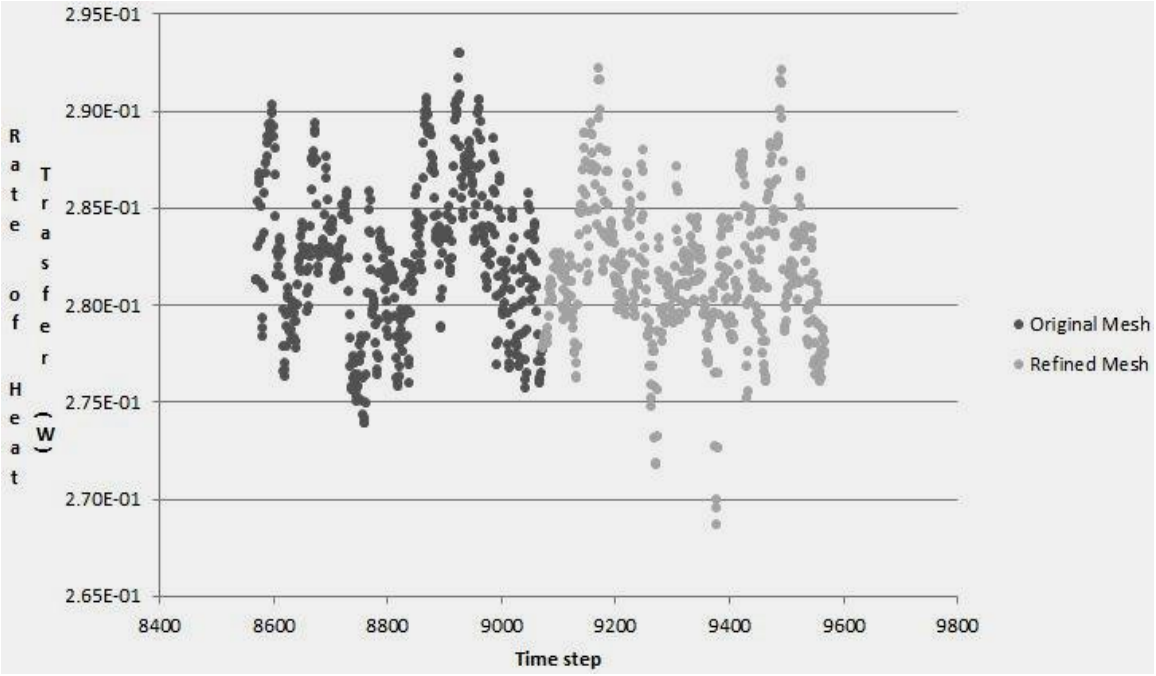

Figure 7: Rate of heat transfer for Case (1) versus simulation timestep. Original and refined meshes are shown.

Boundary conditions for Case (1) are seen in Figures 8 and 9. Figure 8 is an elevation view of the domain, whereas Figure 9 is seen from the plan view. In Figures 8 and 9, it can be seen that the outer boundaries of the fluid domain are specified as entrainment, which is a type of opening. Rather than specify an inlet or an outlet boundary condition, which assumes flow is entirely in or out of the domain on that boundary, entrainment is chosen to let the flow develop naturally. Rotational periodicity is chosen on the symmetry lines seen in Figure 4. A periodic boundary condition assumes that there exists a subdomain which can be repeatedly mirrored to reflect the entire domain. Any fluid leaving the subdomain re-enters at the opposing side. In the present case, the subdomain is the quarter symmetry. In Figure 9, flow exiting one of the periodic boundaries along the axis of the fan re-enters the domain through the opposite periodic boundary. The use of rotational periodicity is justified due to the symmetric nature of the problem.

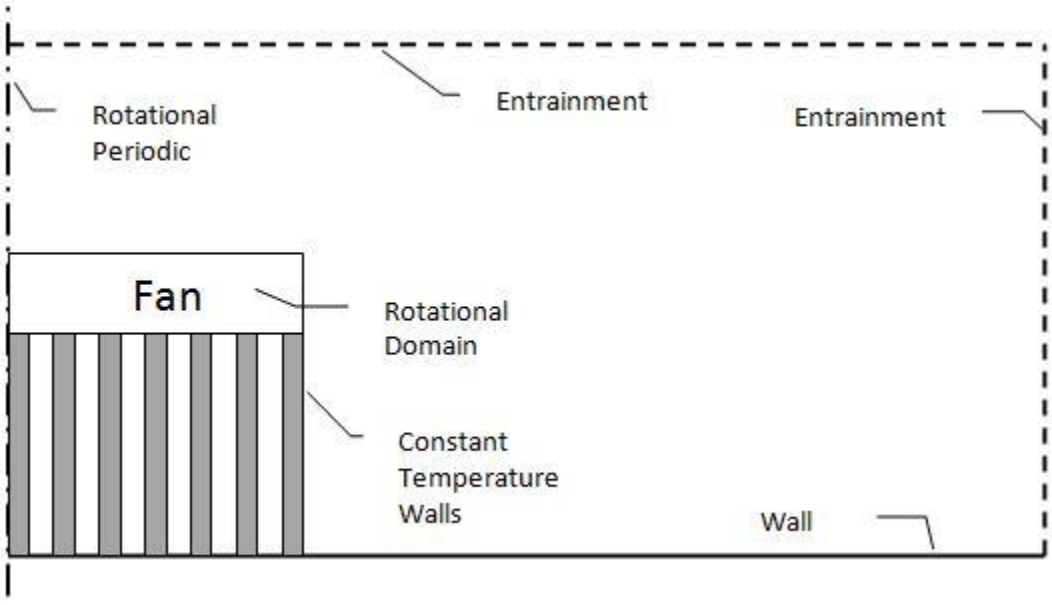

Figure 8: Elevation view of boundary conditions for Case (1).

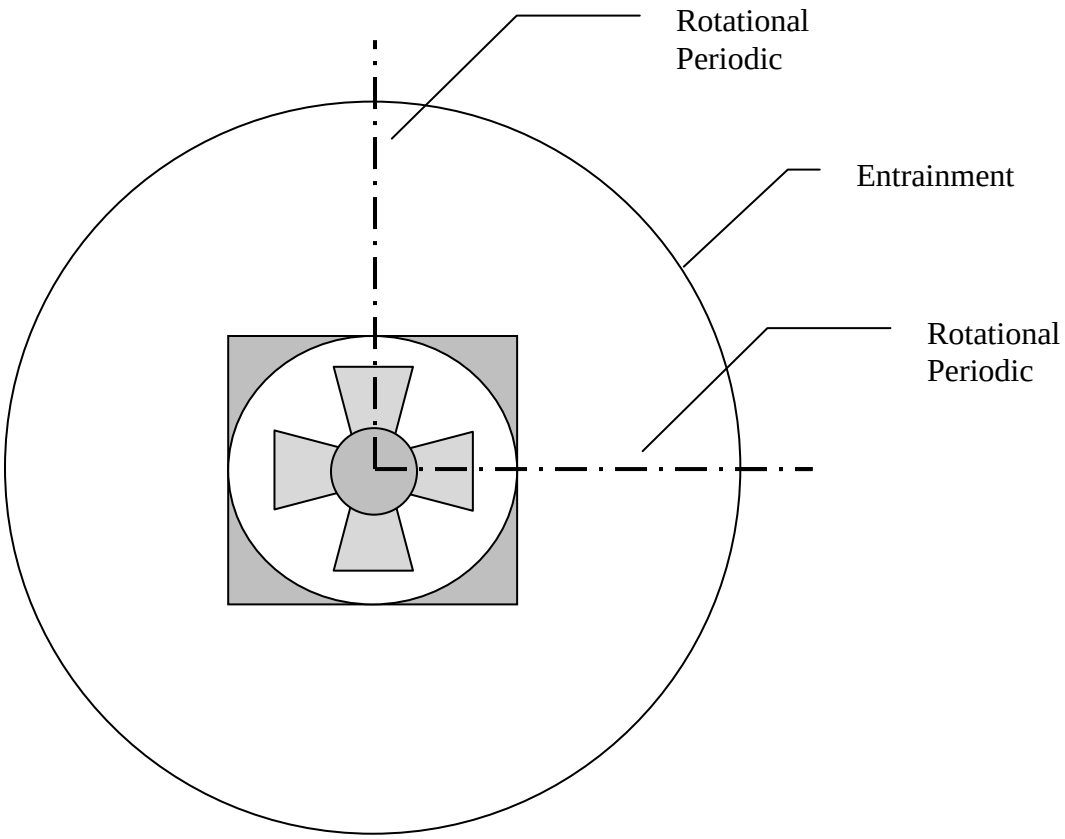

Figure 9: Plan view of boundary conditions for Case (1).

The entire boundary adjacent to the base of the pin fin array is simulated as a no-slip wall. This boundary is chosen to keep the problem as generally applicable as possible. In compact devices, the pin fin array is often attached to a computer chip, which may have various protruding objects (see Figure 1). Any solid objects such as fan blades, fan housing, and pin fins are simulated as no-slip walls. In addition, the pin fins are specified at a constant nondimensional temperature of one. The ambient nondimensional temperature of the fluid in the domain is zero. Nondimensional temperatures are obtained by subtracting the ambient temperature of the fluid and proceeding to divide by the temperature difference of the fins and the ambient.

Governing Equations

The governing equations for this investigation are the mass conservation, momentum conservation, and the turbulence equations. Calculations are performed at every node in the solution domain. The finite-volume method is employed. Conservation of mass can be written in tensor form as,

$$\frac{\partial u_i}{\partial x_i} = 0 \tag{1}$$

The term u_i represents the fluid velocity in the i-th direction. The conservation of momentum equations are expressed as,

$$\rho \frac{\partial u_j}{\partial t} + \rho \left(u_i \frac{\partial u_j}{\partial x_i} \right) = -\frac{\partial p}{\partial x_j} + \frac{\partial}{\partial x_i} \left((\mu + \mu_{turb}) \frac{\partial u_j}{\partial x_i} \right), \quad j = 1,2,3. \tag{2}$$

where the quantity u is the local velocity, ρ is the fluid density, p is the pressure, and μ represents the molecular (dynamic) viscosity. μ_{turb} is the turbulent viscosity which results from local fluctuations in the fluid velocity due to turbulent motion. This term is dealt with using the Shear Stress Transport Model (SST), as first proposed by Menter [11]. The SST Model has proven robust in predicting flow separation, wall shear, and pressure variations in the boundaries of blunt objects, such as the present case of impinging flow onto pin fins. This model combines the prominent κ-ϵ and κ-ω turbulence models. The κ-ϵ model is most successful when used to evaluate free stream regimes, whereas the κ-ω is better suited for handling boundary layers [12-14]. The turbulent viscosity thus is expressed as,

$$\mu_{turb} = \frac{a\rho\kappa}{max(a\omega, SF_2)} \tag{3}$$

Here, κ is the turbulent kinetic energy and ω is the specific rate of turbulent dissipation. Two transport equations are utilized to find these quantities,

$$\frac{\partial(\rho\kappa)}{\partial t} + \frac{\partial(\rho u_i \kappa)}{\partial x_i} = \gamma \cdot P_k - \beta_1 \rho\kappa\omega + \frac{\partial}{\partial x_i}\left[\left(\mu + \frac{\mu_{turb}}{\sigma_k}\right)\frac{\partial\kappa}{\partial x_i}\right] \tag{4}$$

and

$$\frac{\partial(\rho\omega)}{\partial t} + \frac{\partial(\rho u_i \omega)}{\partial x_i} = A\rho S^2 - \beta_2 \rho\omega^2 + \frac{\partial}{\partial x_i}\left[\left(\mu + \frac{\mu_{turb}}{\sigma_w}\right)\frac{\partial\omega}{\partial x_i}\right] \tag{5}$$

$$+2(1-F_1)\rho\frac{1}{\sigma_{w2}\omega}\frac{\partial\kappa}{\partial x_i}\frac{\partial\omega}{\partial x_i}$$

The term γ indicates the degree to which the flow is laminar or turbulent, being closer to zero when the flow is predominately laminar and closer to one when the flow is predominately turbulent. The term P_k represents the rate of turbulence production and is minimized as gamma goes to zero (i.e. the flow becomes laminar). β_1, β_2, and A are experimentally determined. A more thorough review of Eqs. (4) and (5) can be found in Mentor [11].

RESULTS

The results will be presented for each case sequentially, discussing patterns of fluid flow, heat transfer, and temperature distributions. Figure 10 exhibits two of the planes that will be used to display fluid and thermal vectors and contours.

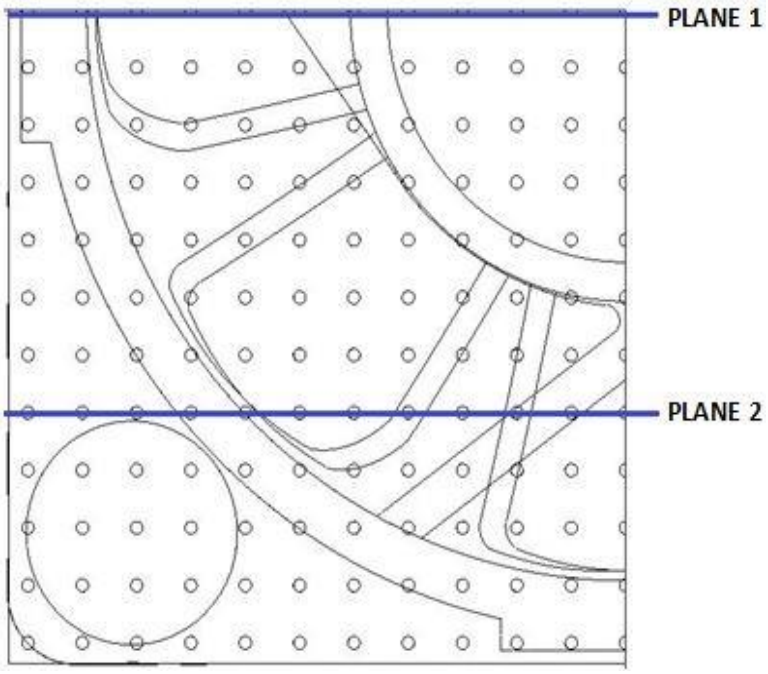

Figure 10: Location of the planes that select data are presented on. Planes bisect the length of the fin.

Case (1): Baseline

A fluid flow vector field of the baseline case is presented in Figure 11. The vectors are on a PLANE 1, as seen in Figure 10, located on one of the lines of geometric symmetry occurring at an instant of time. It should be noted that this problem is transient in nature and the velocity field is changing with time. The vectors represent the fluid velocity tangent to the chosen plane, thus they do not give information about velocity in or out of the plane. The vectors scale in size based upon magnitude of the velocity and are chosen to be equally spaced. As much of the interesting activity is in proximity of the fan and pin fins, Figures 11 and 12 displays only a fraction of the entire fluid domain simulated. In addition to vectors, velocity contours are also included in Figures 13-16. These show

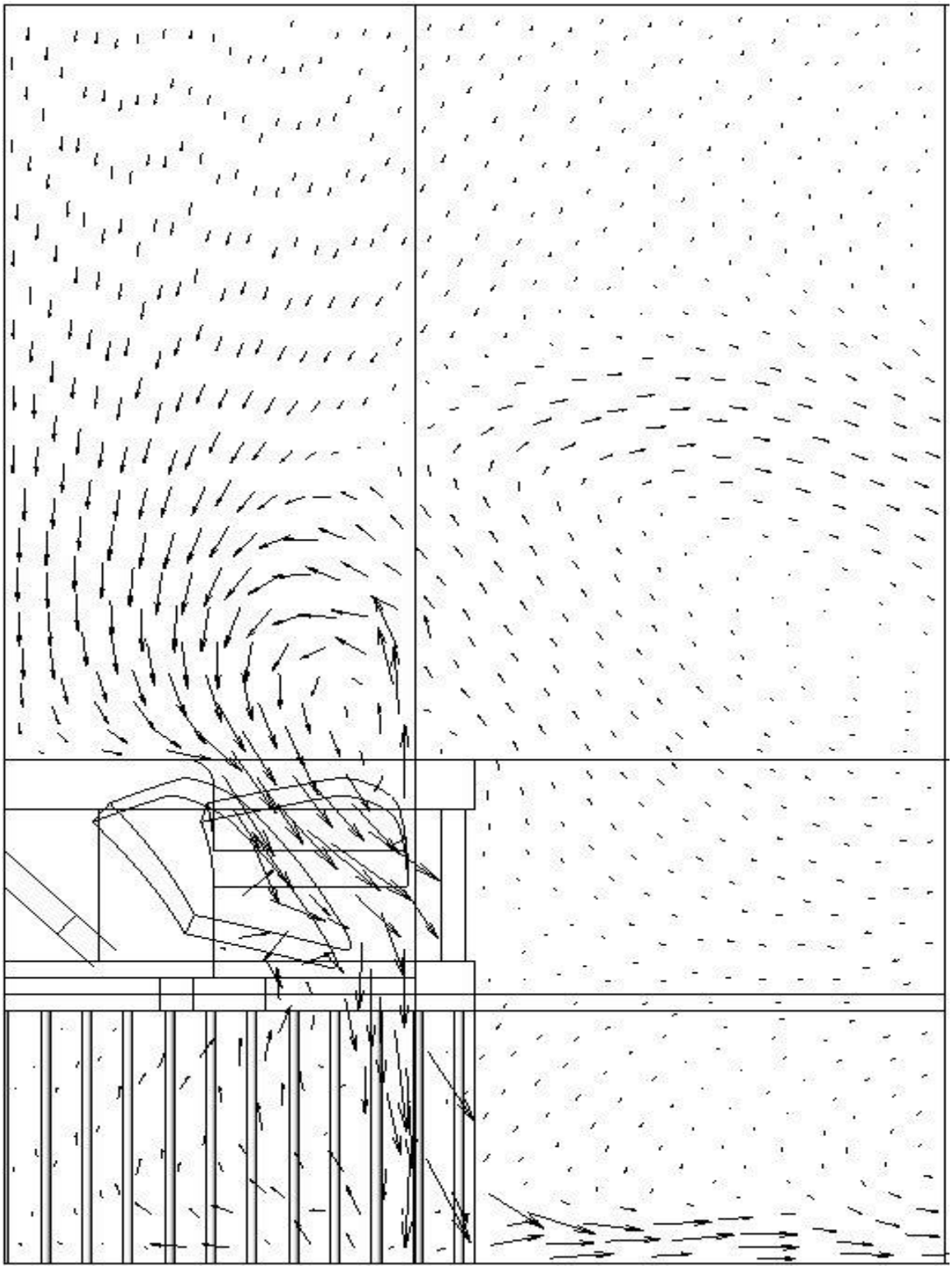

Figure 11: Velocity vector field of Case (1) on PLANE 1.

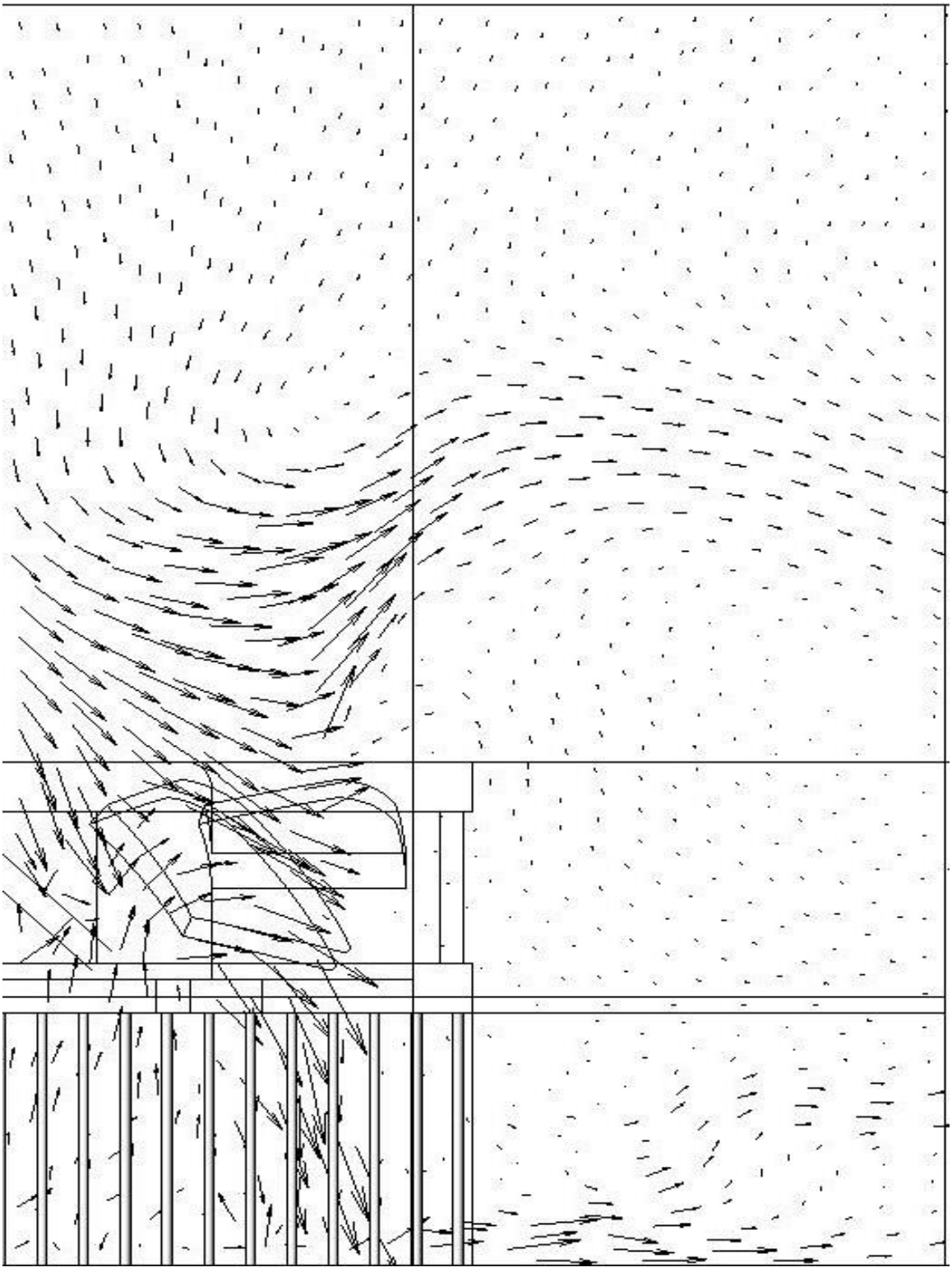

Figure 12: Velocity vector field of Case (1) on PLANE 2.

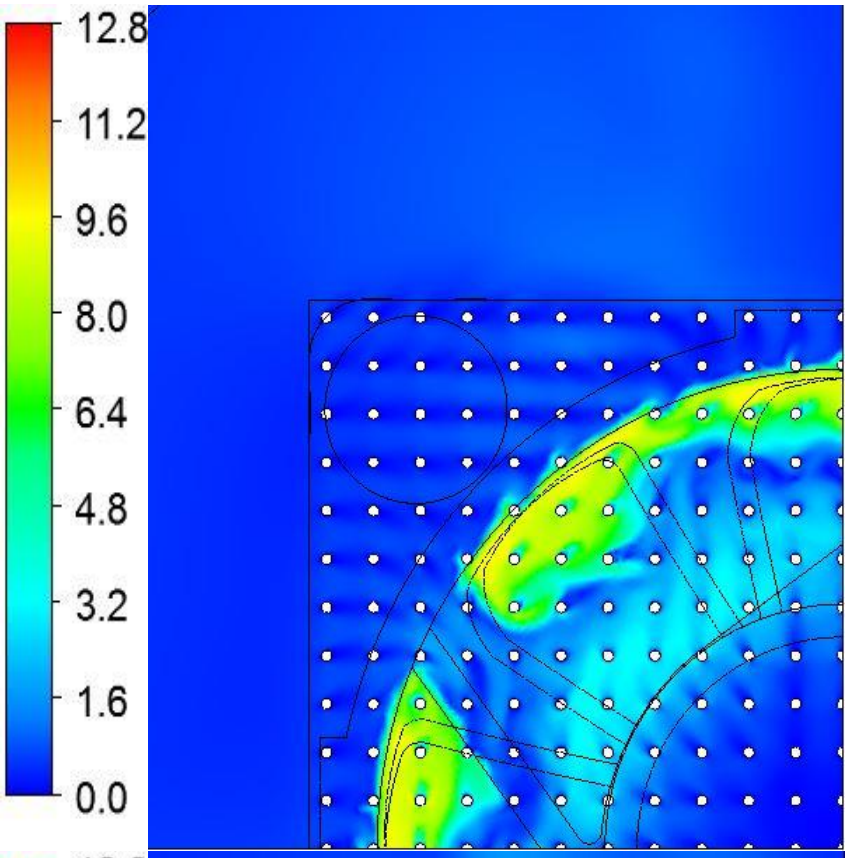

Figure 13: Velocity contour on a plane perpendicular to the axis of the pin fins, located 14 mm from the base of the pin fin array for Case (1).

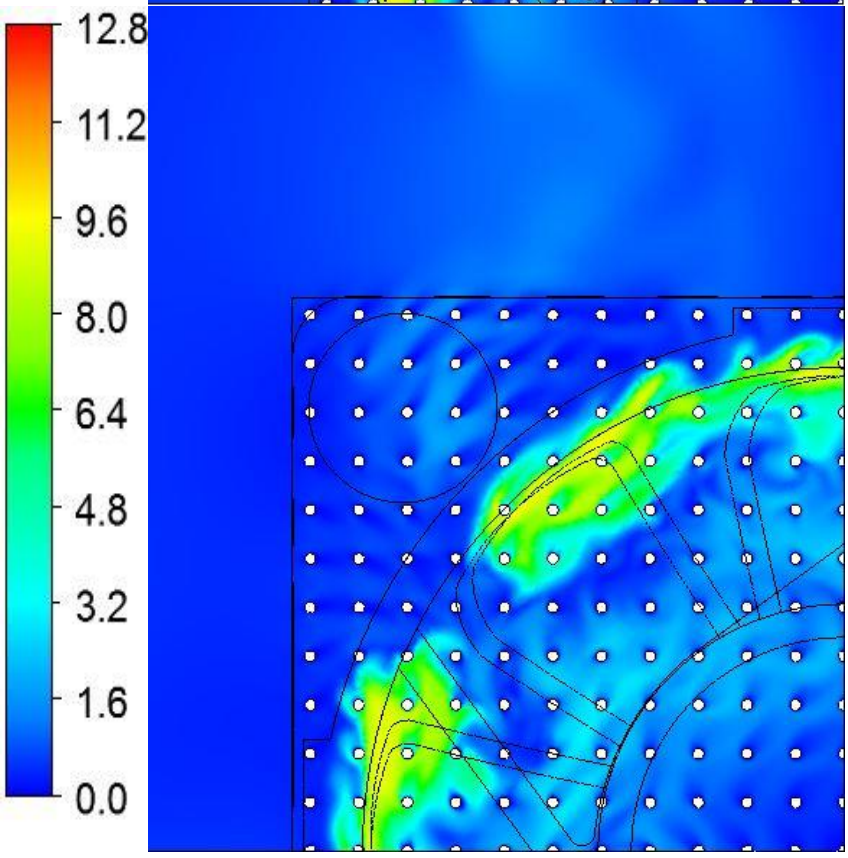

Figure 14: Velocity contour on a plane perpendicular to the axis of the pin fins, located 10 mm from the base of the pin fin array for Case (1).

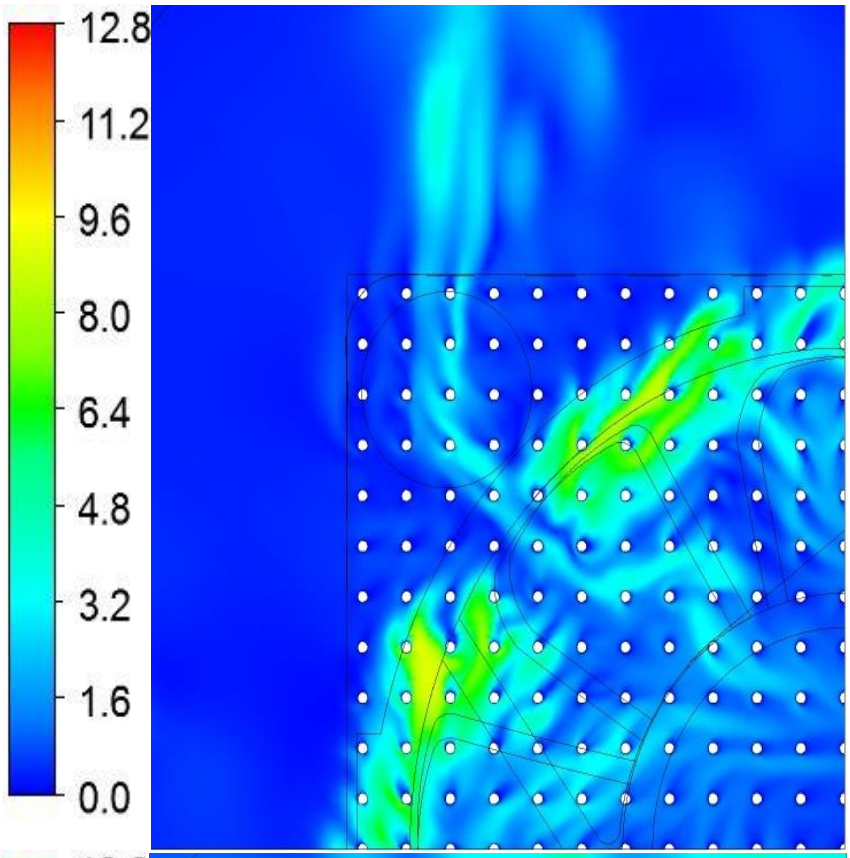

Figure 15: Velocity contour on a plane perpendicular to the axis of the pin fins, located 5 mm from the base of the pin fin array for Case (1).

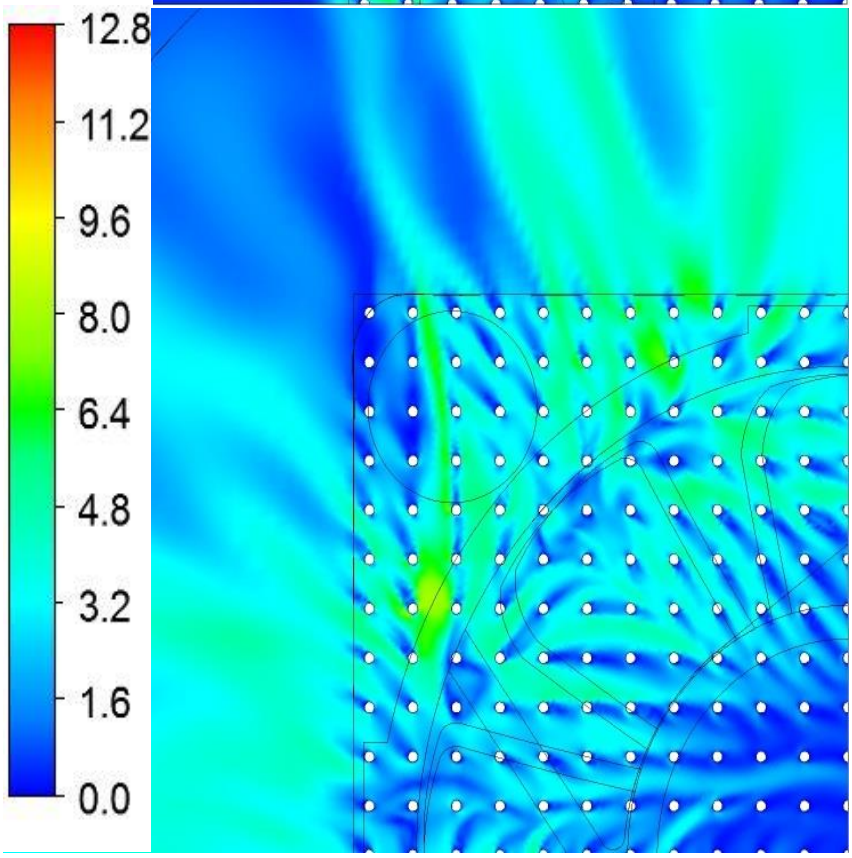

Figure 16: Velocity contour on a plane perpendicular to the axis of the pin fins, located 1 mm from the base of the pin fin array for Case (1).

the magnitude of the three dimensional velocity on planes which bisect the pin fins perpendicularly.

It is clear that the flow is very chaotic in the vicinity of the fan blades and near the fins. Air is pulled into the fan by the rotating blades and a small portion of the flow leaks past the blade tips in the opposite direction, most clearly seen in Figure 11. The rotating blades impart a recirculation zone just upstream of the blades. It can be seen that the largest velocity magnitude occurs near the tips of the fan blades. This high speed air proceeds into the pin fin array and primarily encounters the fins which are in the vicinity of the fan tips. As the air travels farther into the pin fin array it diverges, as seen in Figures 13-16. The air exits the pin fin array at various depths, though primarily the air exits near the base of the pin fin array illustrated clearly by Figures 11 and 16. In Figures 13 and 14, air is seen entering slowly through the left hand side of the array and exiting out the top, corresponding to the direction the blades are rotating. The air beneath the fan housing is fairly stagnant as is evident from Figures 13-16. The air directly beneath the fan hub is also fairly stagnant. Towards the bottom of the pin fin array, the air beneath the housing and fan hub does have some motion. Air beneath the length of the fan blades has a tendency to be pulled out of the pin fin array and back into the fan, as shown by the velocity vectors in Figures 11 and 12. There is a small amount of tip leakage, in which the air travels between the tips of the fan blades and housing backwards toward the inlet. There is minimal amount of recirculation of air exiting the pin fin array back to the inlet of the fan. The most notable findings are that the airflow is greatest at the tips of the fan

blades, the air tends to exit near the base of the pin fin array, air recirculates back into the fan, and air is fairly stagnant beneath the fan hub and housing.

The area integrated heat flux from the pin fin array is computed at each timestep of the simulation, yielding the overall rate of heat transfer. This was previously shown in Figure 7 as a means to compare the original mesh to the refined mesh for the baseline case. The rate of heat transfer is important, as it indicates the ability of the heat sink to dissipate thermal energy. It is useful to calculate the time averaged rate of heat transfer. This is easily obtained by averaging the rate of heat transfer found at each timestep. The average rate of heat transfer for the all of the investigated cases are listed in Table 4. Note that this is for the entire geometry, not just the quarter simulated.

One objective of this study is to investigate which fins are best or worst at transferring heat, as opposed to just computing the overall rate of heat transfer. This is done by computing the rate of heat transfer from each pin fin and nondimensionlizing it by the time averaged rate of heat transfer of a fin. The time averaged value is chosen due to accuracy. For instance, imagine if the average rate of heat transfer was computed based upon only one timestep. If the sample timestep chosen was at a peak or trough seen in Figure 7, this would give an inaccurate representation of what the typical rate of heat transfer is. Figure 17 displays the rate of heat transfer of a given pin fin divided by the time averaged rate of heat transfer for the average fin. This ratio yields a dimensionless quantity which indicates how well the pin fin dissipates thermal energy. The X and Y axes represent the column and row of the heat sink array respectively. Each circle represents a pin fin at specified X and Y coordinates. Notice that the size the circles

vary. Larger circles indicate a higher rate of heat transfer, whereas smaller circles indicate a lower rate of heat transfer. A legend is provided in the figure. The numerical value is the ratio of heat transfer rate to time averaged heat transfer rate and is included below each pin fin. The position of the fan blades, hub, and housing in the quarter symmetry can be seen in Figure 17(b), included separately to reduce cluttering in the figure.

It can be seen that the lowest heat transfer for the fin array occurs in the upper right corner of Figure 17(a). This region is directly beneath the fan hub, as is seen in Figure 17(b). The lowest dimensionless heat transfer ratio is a mere 0.03, indicating that heat transfer from pin fins from this region is much lower than the average pin fin. This is due to the hub blocking airflow creating a semi-stagnant fluid region. Moving away from the hub radially, the heat transfer becomes better and the dimensionless heat transfer ratio begins to approach unity. Recall that the air in this region has a tendency to be recirculated into the fan, as is seen in Figures 11 and 12.

Moving out slightly farther radially, the region of best heat transfer is observed. Values in this range are well above unity and even approach 3.0. This corresponds to the region which is in line with the ends of the fan blades. Recall that the air is at its greatest speed at the end of the fan blades, as is observed in Figures 11-14. Viewing the regions outside the tips of the fan blades and directly under the fan housing, it is seen that the dimensionless heat transfer ratio decreases. The ratio is around or below unity in the lower left corner of Figure 17(a). This decrease is due to the flow blockage presented by

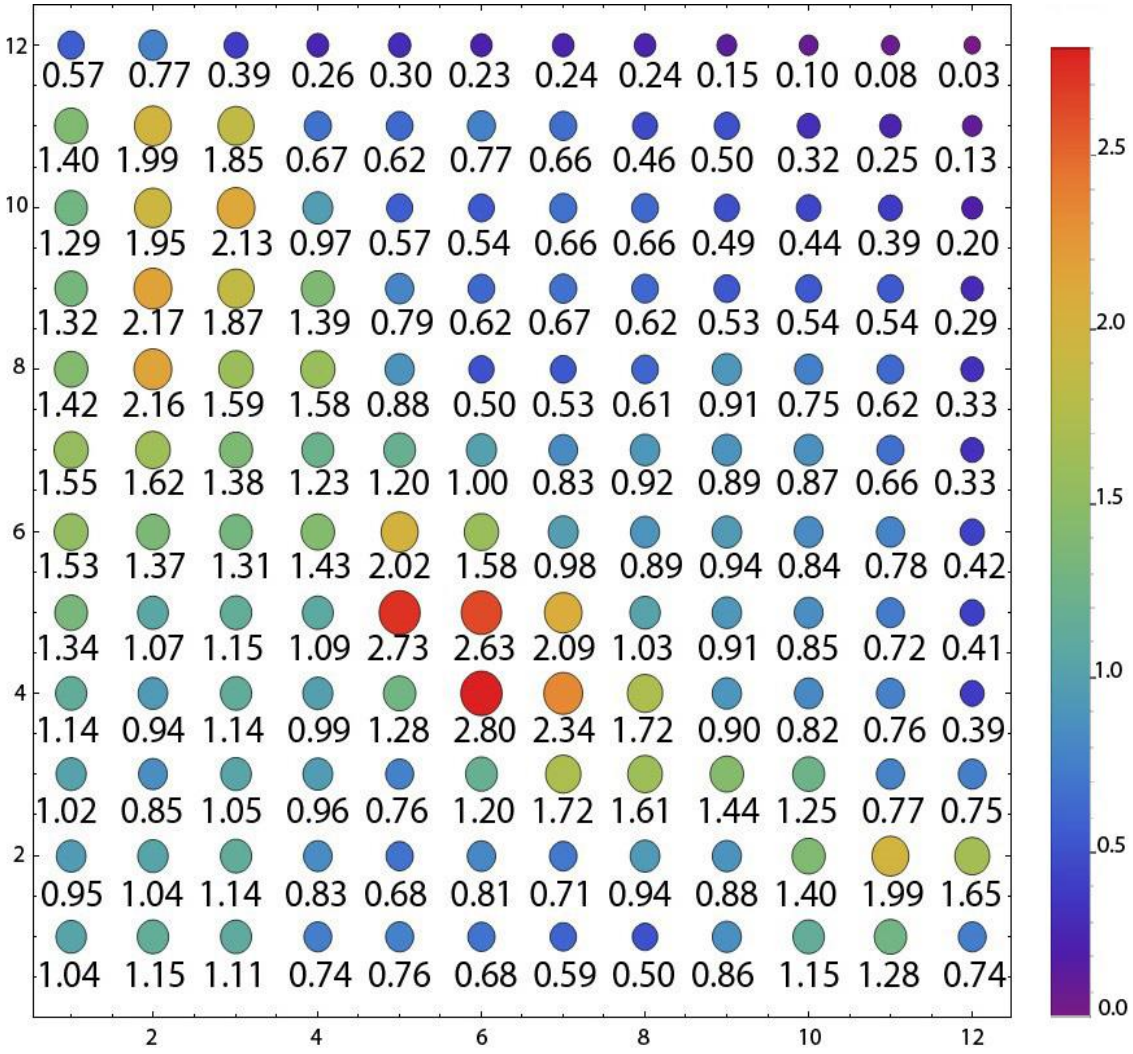

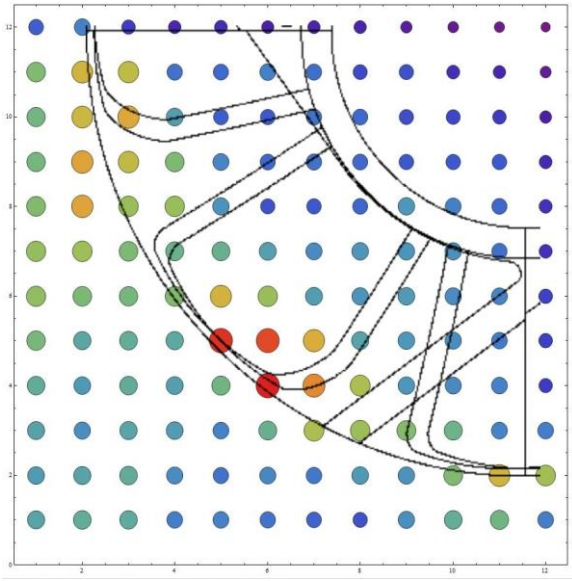

Figure 17: Rate of heat transfer of a given pin fin divided by the time averaged rate of heat transfer of the average fin for Case (1). This ratio is a dimensionless quantity indicating the effectiveness of a given fin at dissipating thermal energy. See text for a detailed description.
(a). The top image is a numerical representation of the ratio.
(b). The bottom image displays the location of the fan, hub, and housing.

the housing of the fan. Notice that the values in the upper left region of Figure 17(a) are higher than those in the lower right region. In fact, one might expect the values to be fairly similar along the whole region in line with the tips of the fan blades. Less airflow travels along the fins in the lower right region of Figure 17 and instead travels in the neighboring region where heat transfer is highest due to the blockage presented by the small piece of housing which connects the fan hub to the housing (see 17(b) or Figure 3 to view this piece). Such a blockage is not present near the fins in the upper left region of Figure 17. This demonstrates the magnitude of the impact that blockages present on the airflow and thus the heat transfer.

Temperature contours of the pin fin array and fan presented in Figures 18-23. Figures 18 and 19 exist on PLANE 1 and PLANE 2 respectively. Figures 20-23 correspond to the same locations as the velocity contours seen in Figures 13-16. The ambient temperature is zero and the temperature of the fins is one, obtained by subtracting the ambient temperature and proceeding to divide by the temperature difference of the fins and the ambient.

It is seen that the air entering the fan is very near ambient temperature. It was mentioned when discussing the velocity field that tip leakage was observed. This is indicated in Figures 18 and 19 by the slightly higher than ambient temperature which is expanding backwards out of the inlet. Moving into the fan and pin fin array, it is seen that there exists a region that has cooler temperatures. This region corresponds to the high air

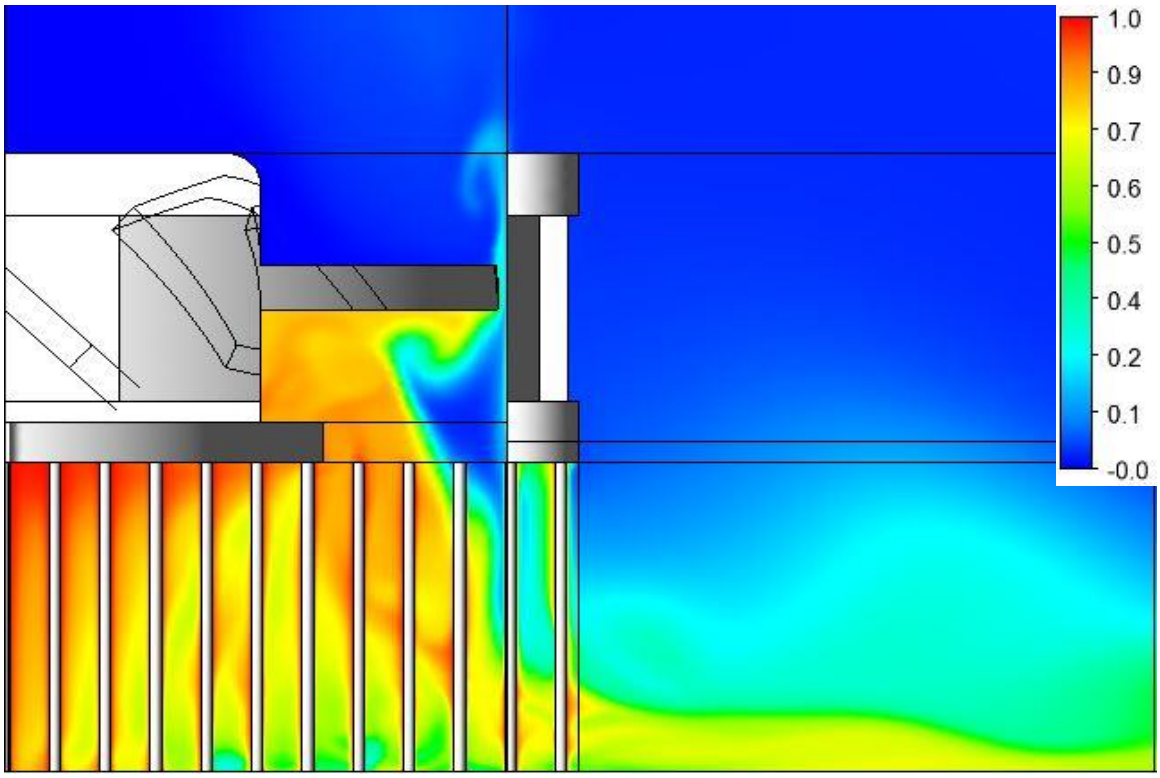

Figure 18: Temperature contour of Case (1) on PLANE 1.

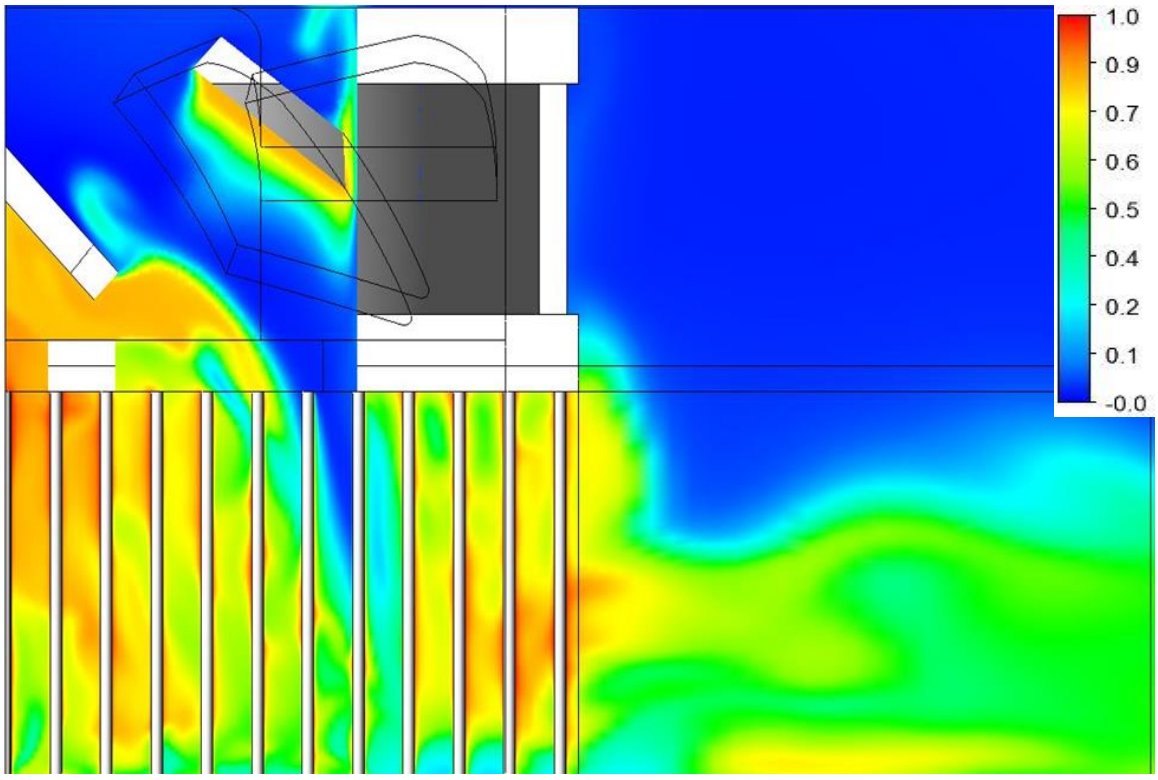

Figure 19: Temperature contour of Case (1) on PLANE 2.

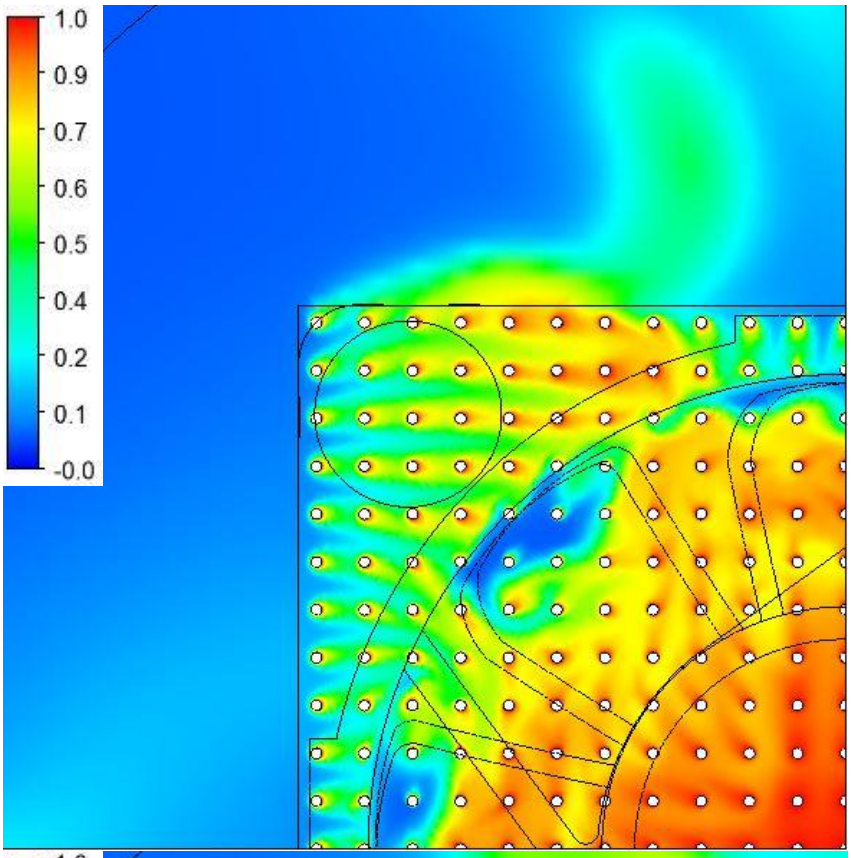

Figure 20: Temperature contour on a plane perpendicular to the axis of the pin fins, located 14 mm from the base of the pin fin array for Case (1).

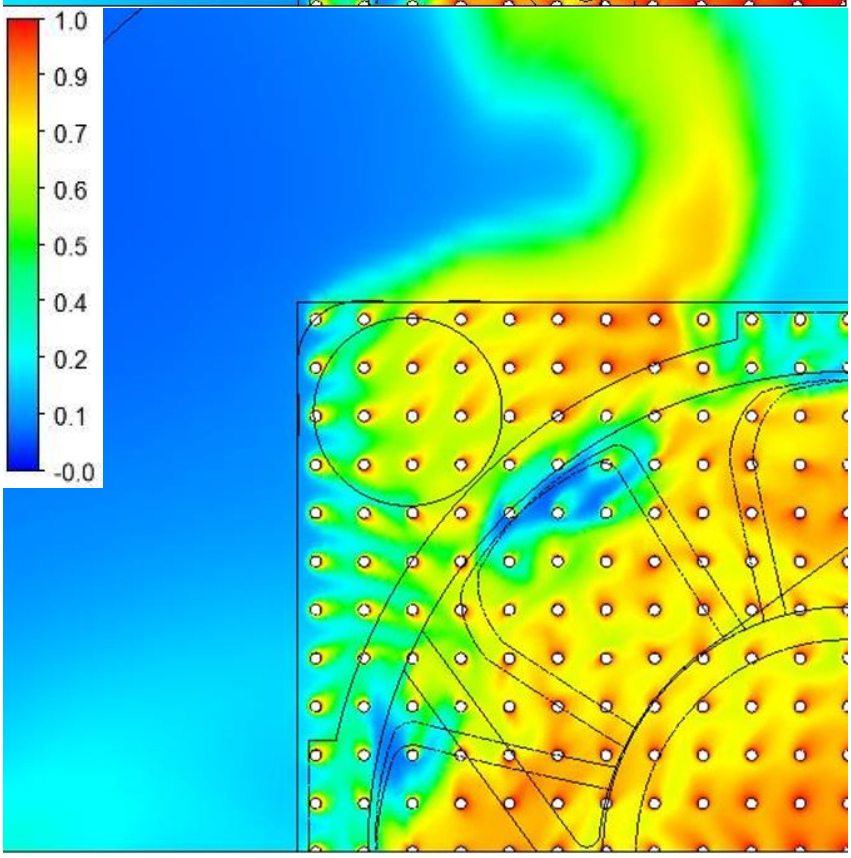

Figure 21: Temperature contour on a plane perpendicular to the axis of the pin fins, located 10 mm from the base of the pin fin array for Case (1).

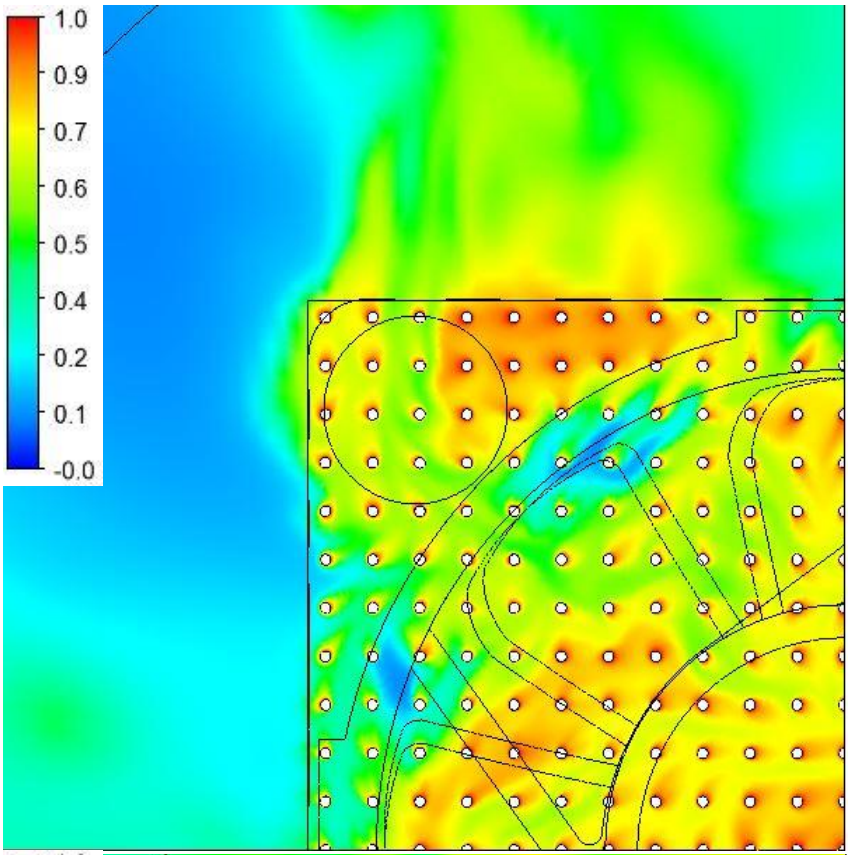

Figure 22: Temperature contour on a plane perpendicular to the axis of the pin fins, located 5 mm from the base of the pin fin array for Case (1).

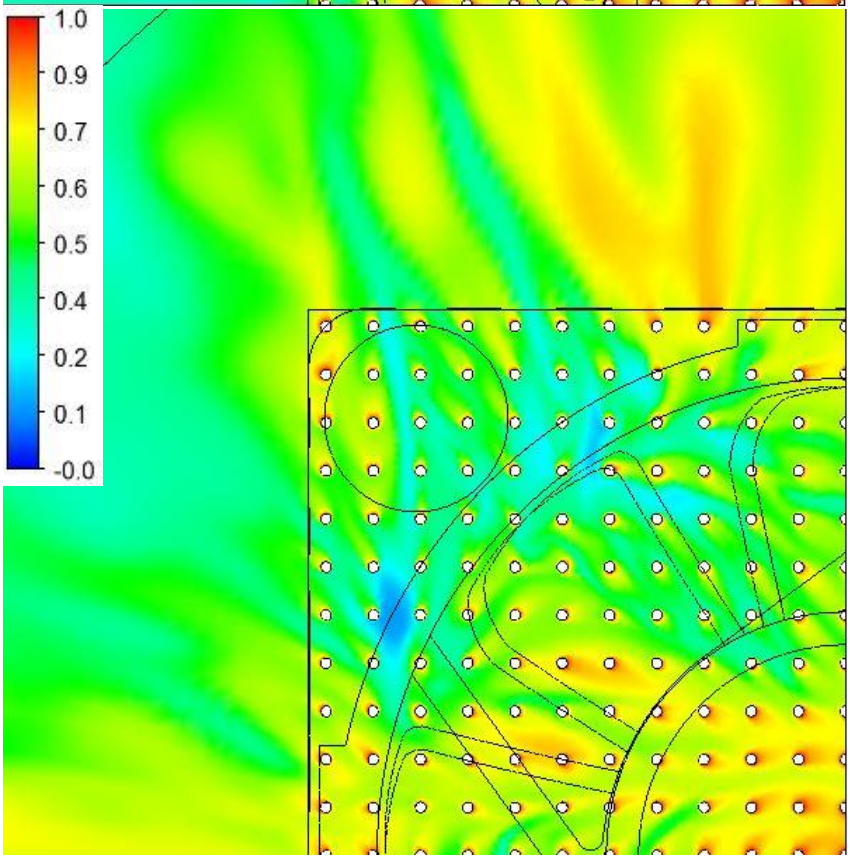

Figure 23: Temperature contour on a plane perpendicular to the axis of the pin fins, located 1 mm from the base of the pin fin array for Case (1).

speed region clearly shown in Figures 11 and 12. The fluid temperature is lower here due to convection. From Figures 20-23, it is clear that air impinges onto the fins most strongly in the region in line with the tips of the fan blades. Air continues down to the base of the heat sink, diverging and cooling the array as it travels. Air can be seen to be entering the left hand side of the array and exiting out the top side of the array in Figures 20 and 21 due to the direction the blades are rotating. In Figure 23, the air at the edge of the heat sink can be seen rushing out in all directions. Air in the center of the array is more chaotic, but has a tendency to recirculate back into the fan. This recirculated heat is seen in Figures 18 and 19. The regions beneath the fan housing and hub remain hotter than the rest of the pin fin array. This corresponds to the limited airflow in these regions seen in Figures 11-16.

Case (2)

Case (2) is fan-driven impinging flow on 15 mm pin fins, with a constant temperature heat sink base equal to the temperature of the fins. All of the parameters and the geometry are the same as in Case (1), except the base of the pin fins is no longer adiabatic. A fluid flow vector field of Case (2) is presented in Figure 24. This figure is on PLANE 1, shown in Figure 10. It can be seen that the fluid flow is very similar to Case (1), seen in Figure 11. This is expected since the only difference between the two cases is a boundary condition. Other velocity diagrams are omitted due to the similar nature of the flow. The most notable features of the velocity

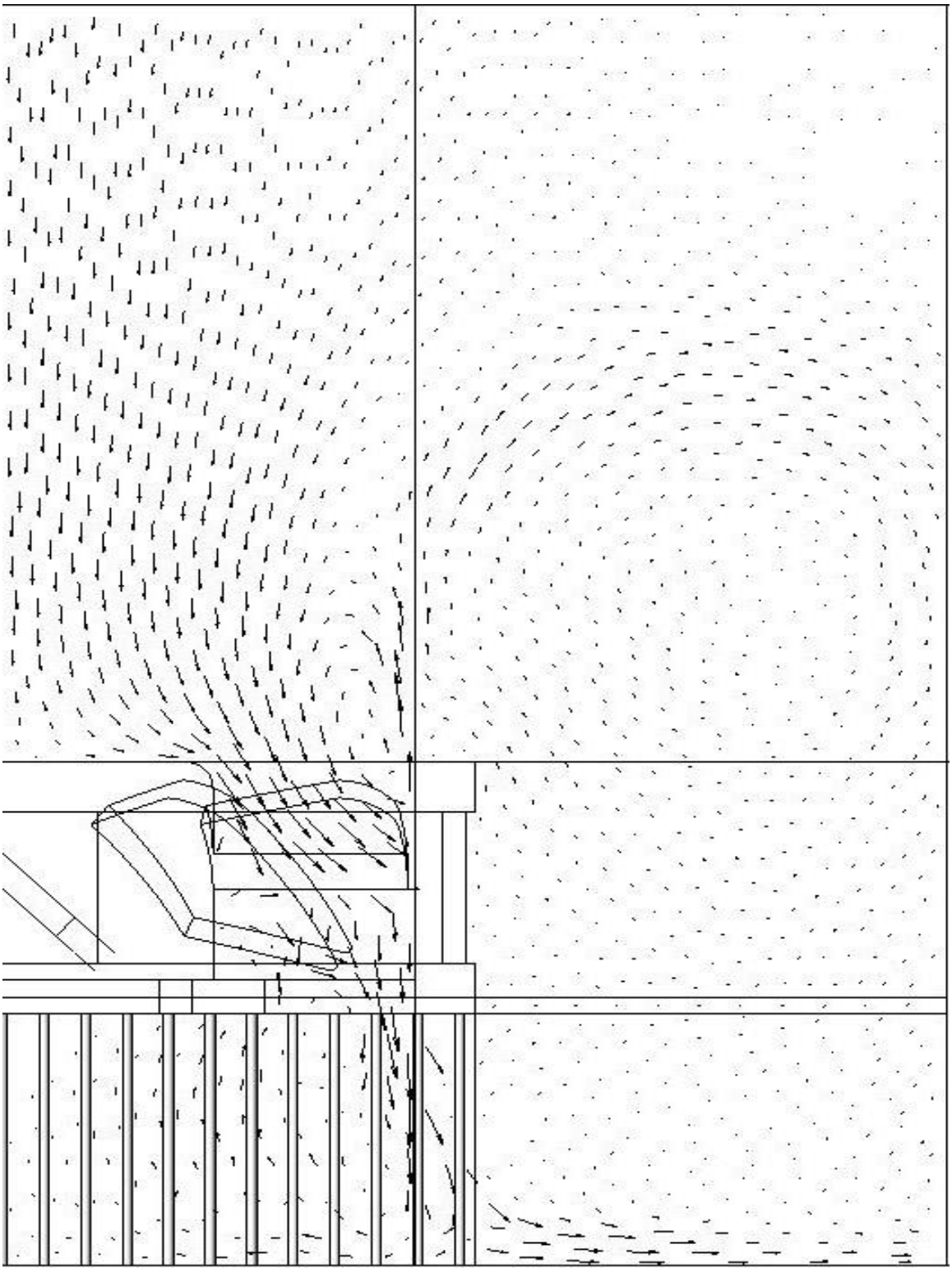

Figure 24: Velocity vector field of Case (2) on PLANE 1.

field are low air speeds underneath the fan hub and housing, high speeds at the tips of the fan blades, and recirculation of the fluid both at the inlet and outlet of the fan.

The dimensionless heat transfer ratio of each fin in Case (2) can be seen in Figure 25(a). This figure demonstrates that the pin fins responsible for the greatest and least amount of heat transfer remain the same as Case (1). Pin fins underneath the hub contribute very little to the overall heat transfer from the array, whereas pin fins along the region in line with the fan blade tips contribute the most. It is meaningless to compare numerical values of the dimensionless heat transfer ratio between cases as the problem is transient in nature. However, it is seen that the general trends noted hold throughout time.

A temperature contour of Case (2) is shown in Figure 26. Similar to Case (1), the coolest regions correspond to the fins in line with the tips of the fan blades, where high speed air impinges. Hot regions are still found beneath the fan hub and housing. Flow tends to exit near the base of the pin fin array, though some exits elsewhere. Air is recirculated back into the fan from the central region of the pin fin array, as was seen in Case (1). The most dramatic differences between Case (1) and Case (2) are seen in Figure 26. Temperatures in the pin fin array are overall higher in Case (2) than Case (1). This is especially evident when viewing the air beneath the fan hub, which is very near the constant fin temperature. Recall that air is fairly stagnant beneath the hub, as is evident from Figures 11-16. Interestingly, the air in the high speed flow region is still very near ambient temperature and does not seem to be affected by the contribution of the pin fin base. Overall heat transfer of the pin fins is around 94% of Case (1), as is seen in Table 4.

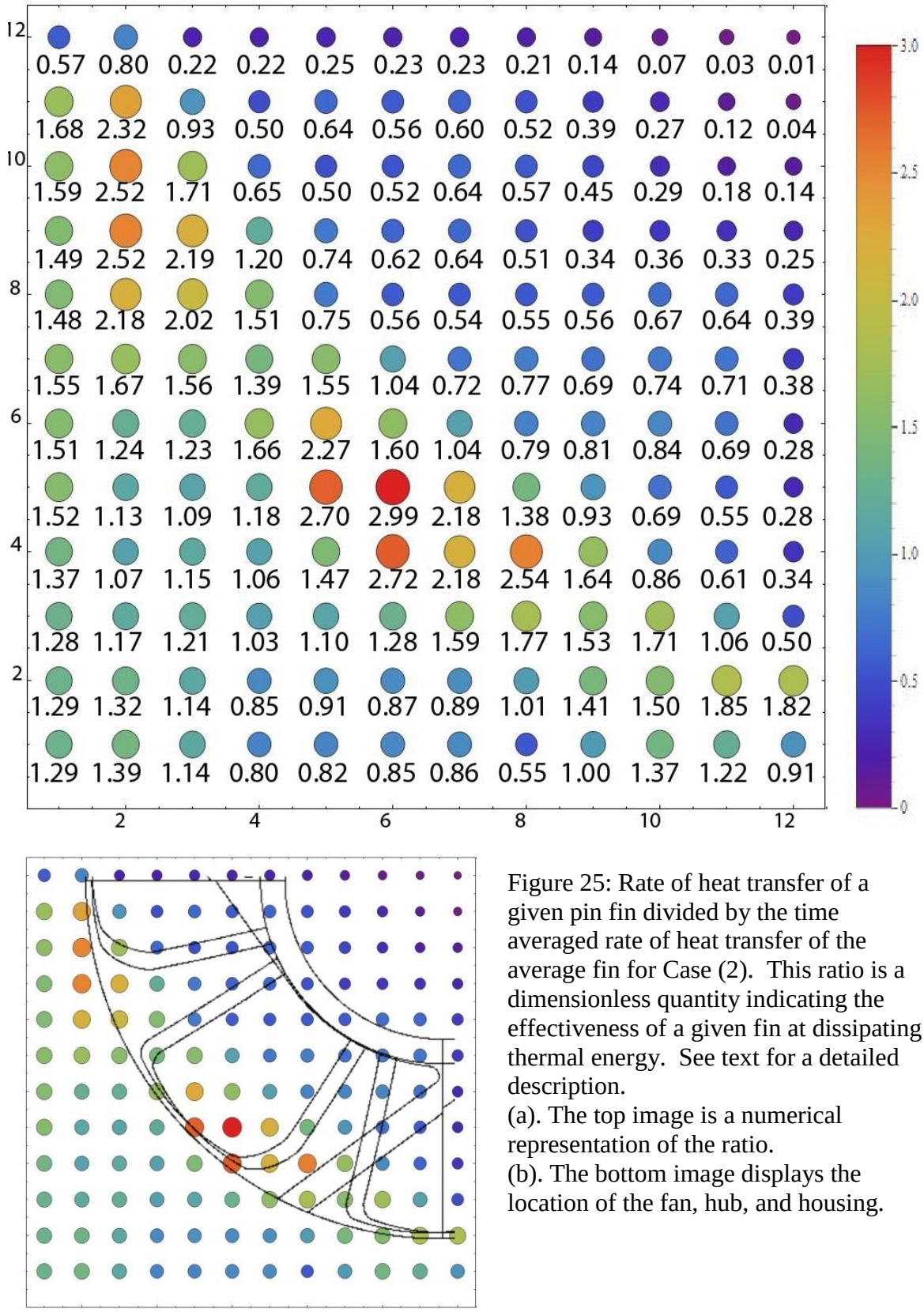

Figure 25: Rate of heat transfer of a given pin fin divided by the time averaged rate of heat transfer of the average fin for Case (2). This ratio is a dimensionless quantity indicating the effectiveness of a given fin at dissipating thermal energy. See text for a detailed description.
(a). The top image is a numerical representation of the ratio.
(b). The bottom image displays the location of the fan, hub, and housing.

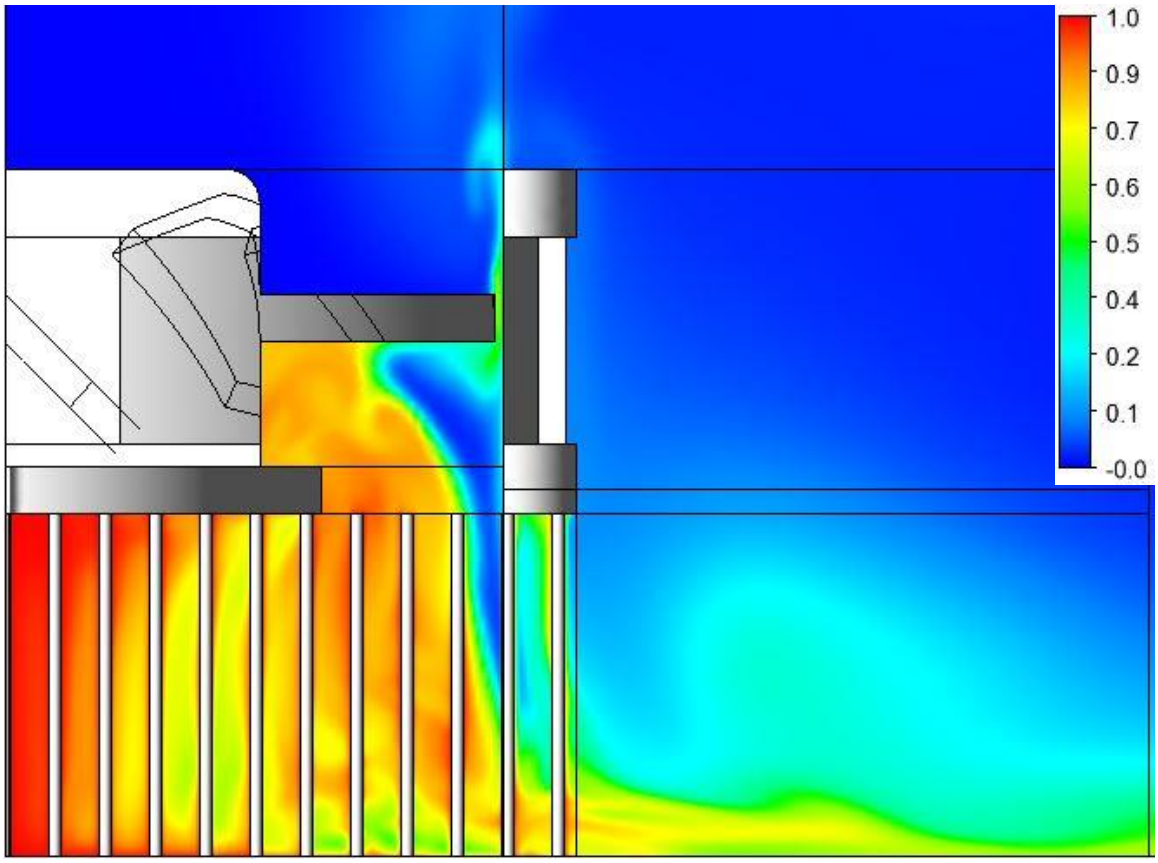

Figure 26: Temperature contour of Case (2) on PLANE 1.

Case (3)

Case (3) is fan-driven impinging flow on 25 mm pin fins. All parameters and the geometry are the same as in Case (1), except the pin fins have been extended by 10 mm. A velocity vector field of Case (3) is presented in Figure 27. This figure is on PLANE 1, shown in Figure 10. It can be seen that the fluid flow is similar to Case (1), seen in Figure 11, most notably low air speeds underneath the fan hub and housing, high speeds at the tips of the fan blades, and recirculation of the fluid both at the inlet and outlet of the fan. A major concern is whether the air penetrates the full depth of the pin fin array due

to convection being the primary mode of heat transfer. In Case (1), it was seen in Figure 16 that some of the air fully penetrated the pin fin array. A similar velocity contour is seen in Figure 29, which is located 1 mm from the base of the pin fin array. This shows that air still readily penetrates the pin fin array. However, note that the magnitudes of the velocities are higher in Case (1) than in Case (3) at 1 mm from each base. Figure 28 shows a velocity contour which is 11 mm from the base of the pin fin array or 14 mm from the outlet of the fan. This figure on a plane equal distance from the outlet of the fan as seen in Figure 16 of Case (1). Figure 28 demonstrates the differences in the velocity field between Case (1) and Case (3) at a given location.

The dimensionless heat transfer ratio of each pin fin in Case (3) can be seen in Figure 30(a). This figure demonstrates that the pin fins responsible for the greatest and least amount of heat transfer remain similar to Case (1). It is noteworthy that the fins beneath the fan hub seem to contribute even less to the overall heat transfer than in Case (1). This is attributed to the fins being 10 mm longer. Having longer fins (i.e. more surface area) in the higher airflow regions results in more heat transfer via convection, however the same is not true beneath the hub where the air has little motion. This yields a higher average and lower or higher ratios as a result.

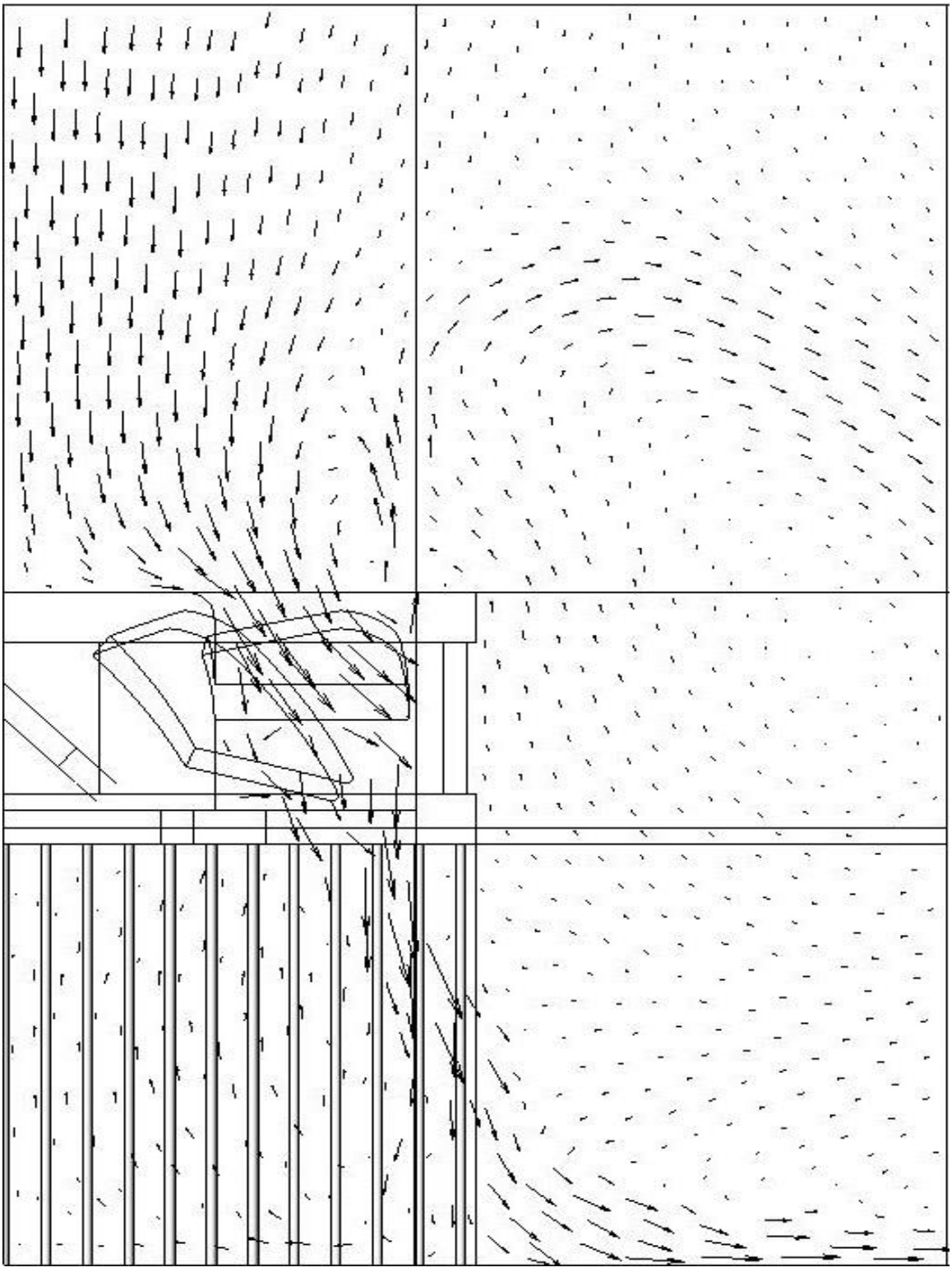

Figure 27: Velocity vector field of Case (3) on PLANE 1.

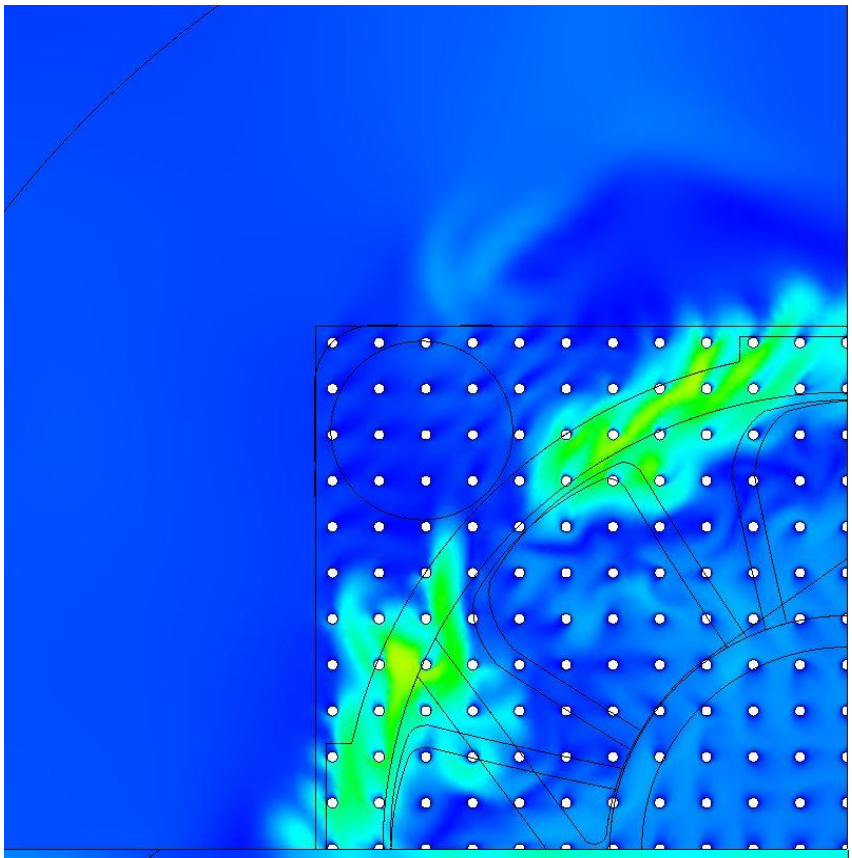

Figure 28: Velocity contour on a plane perpendicular to the axis of the pin fins, located 11 mm from the base of the pin fin array and 14 mm from the outlet of the fan for Case (3).

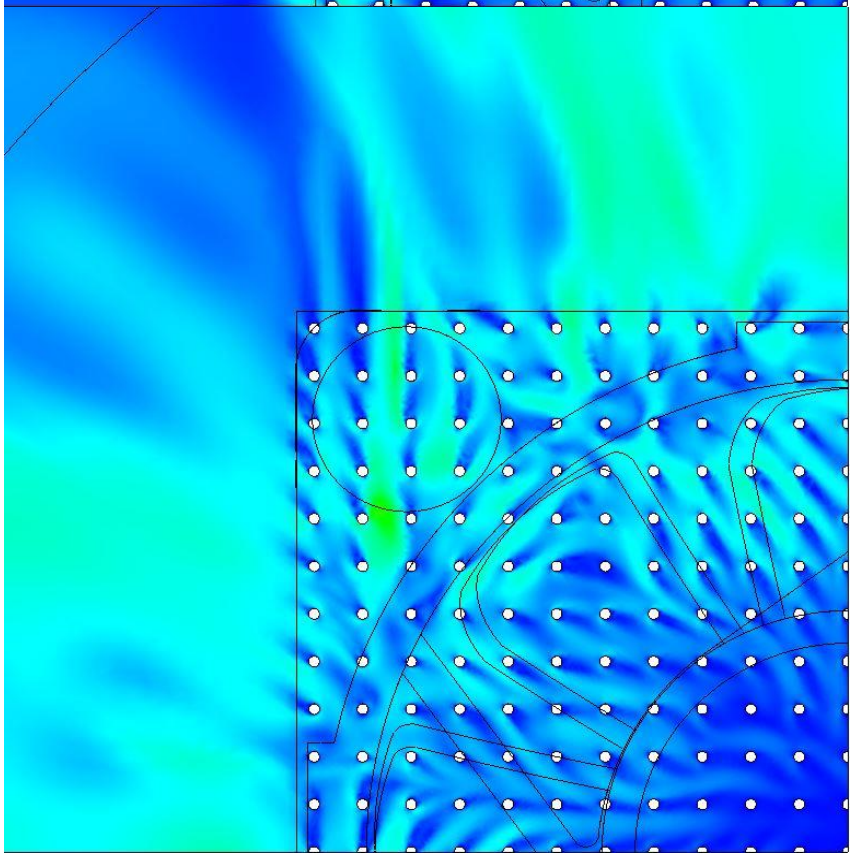

Figure 29: Velocity contour on a plane perpendicular to the axis of the pin fins, located 1 mm from the base of the pin fin array for Case (3).

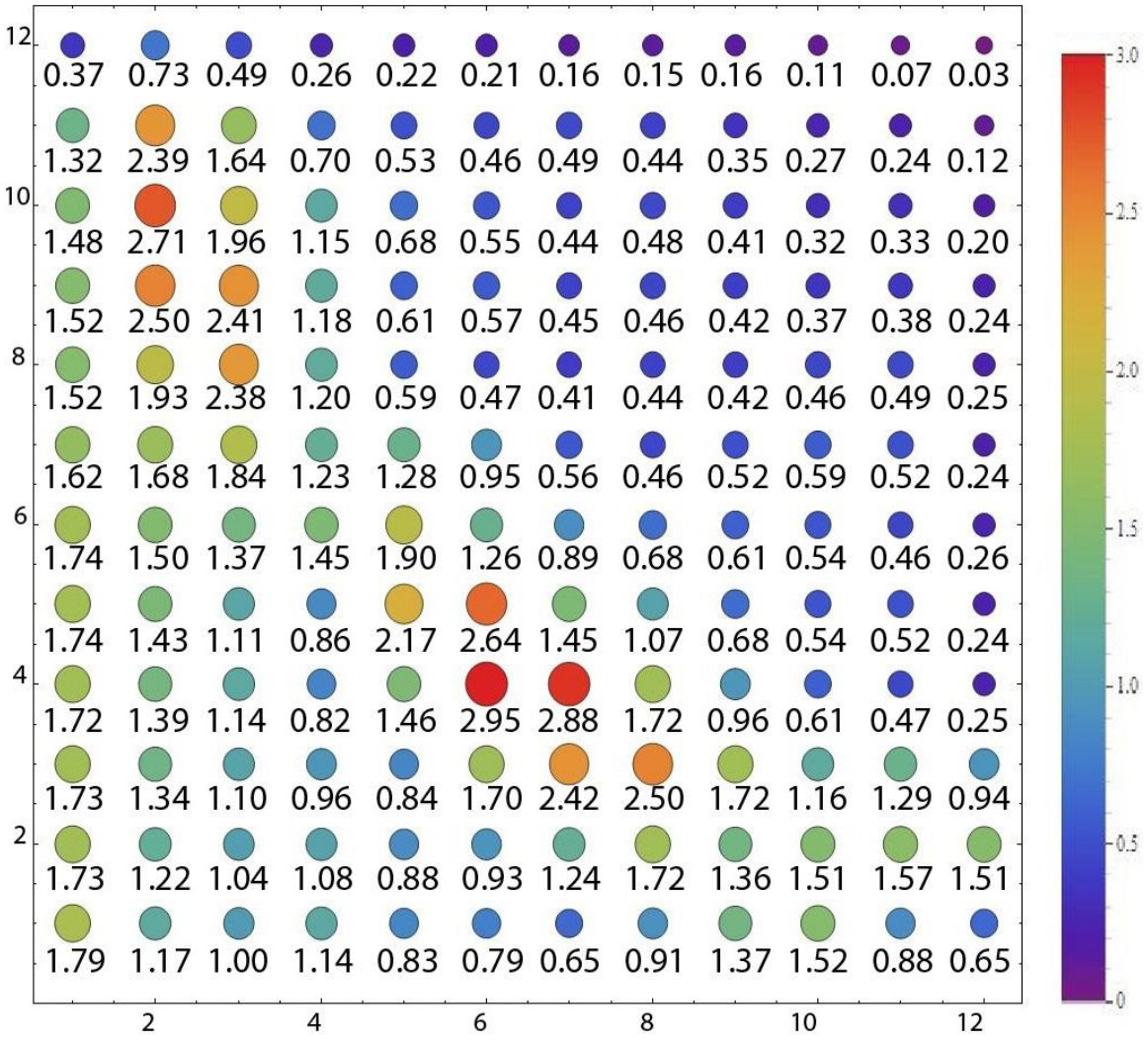

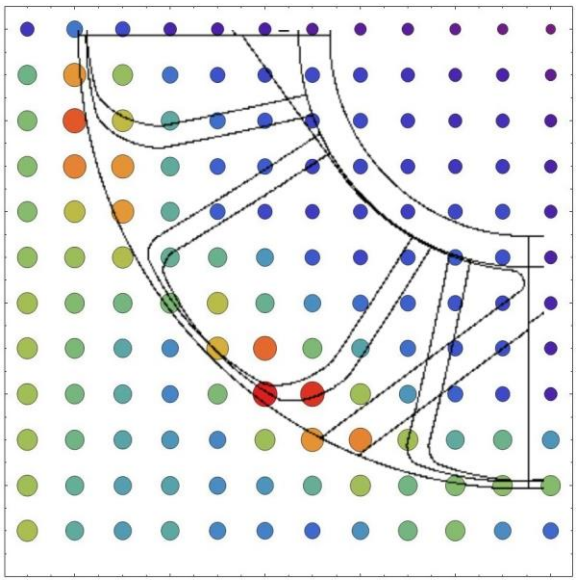

Figure 30: Rate of heat transfer of a given pin fin divided by the time averaged rate of heat transfer of the average fin for Case (3). This ratio is a dimensionless quantity indicating the effectiveness of a given fin at dissipating thermal energy. See text for a detailed description.
(a). The top image is a numerical representation of the ratio.
(b). The bottom image displays the location of the fan, hub, and housing.

A temperature contour of Case (3) on PLANE 1 is shown in Figure 31. Similar to Case (1), the coolest region in the pin fin array corresponds to the top of the fins in line with the tips of the fan blades, where high speed air impinges. The hottest regions are still found beneath the fan hub and housing. Flow tends to exit at toward the base of the pin fin array. Temperatures in the pin fin array are higher in Case (3) than in Case (1). This is due to increased heat input and decreased fluid motion within the pin fin array. Interestingly, hot air is seen to be traveling along the outer housing of the fan and back through the fan inlet. Overall heat transfer of the pin fins is around 126% of Case (1), as is seen in Table 4.

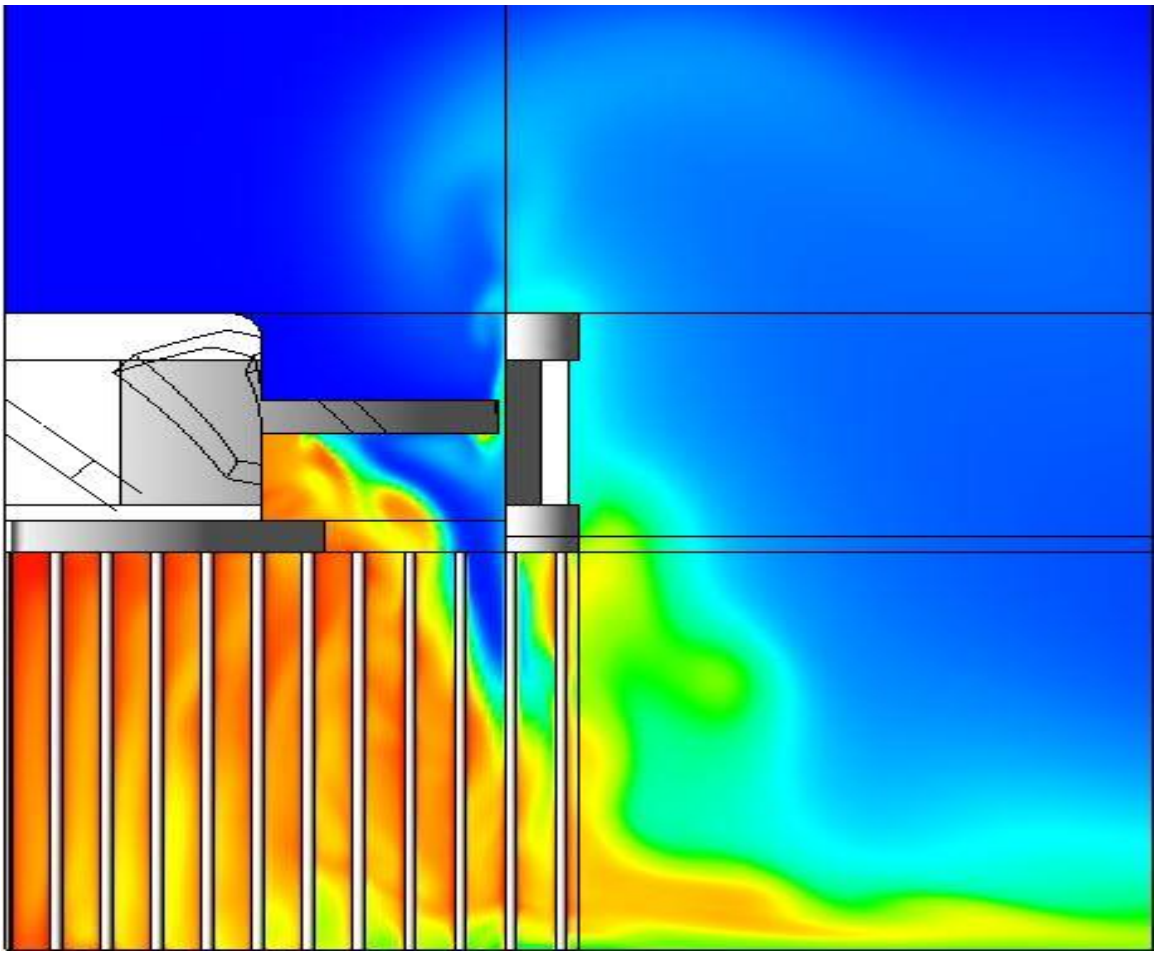

Figure 31: Temperature contour of Case (3) on PLANE 1.

Case (4)

Case (4) is fan-driven impinging flow on 15 mm pin fins, with a shroud placed on the housing of the fan. All of the parameters and the geometry are the same as in Case (1), except for the addition of a shroud. A fluid flow vector field of Case (2) is presented in Figure 32. This figure is on PLANE 1, shown in Figure 10. It can be seen that the fluid flow is very similar to Case (1), seen in Figure 11. Note that there is a thin, rectangular region extending out from the housing with no fluid vectors crossing it. This region represents the shroud. Other velocity diagrams are omitted due to the similar nature of the flow to Case (1). The most notable features of the velocity field are low air speeds underneath the fan hub and housing, high speeds at the tips of the fan blades, and recirculation of the fluid both at the inlet and outlet of the fan. The primary differences between Case (4) and Case (1) are lower air speeds along the shroud, due to the no-slip boundary and lower air speeds around the outer housing of the fan. These lower speeds are a result of air not being allowed to recirculate from the exit of the fan back to the inlet.

The dimensionless heat transfer ratio of each fin in Case (4) can be seen in Figure 33(a). This figure demonstrates that the pin fins responsible for the greatest and least amount of heat transfer are similar to Case (1). Pin fins underneath the hub contribute very little to the overall heat transfer from the array, whereas pin fins along the region in line with the fan blade tips contribute the most. Interestingly, in the upper left corner of Figure 33(a), the pin fins in line with the tips of the fan blades have a similar heat transfer ratio as the pin fins in line with the tips of the fan blades in the center. Recall, in Figure 17(a)

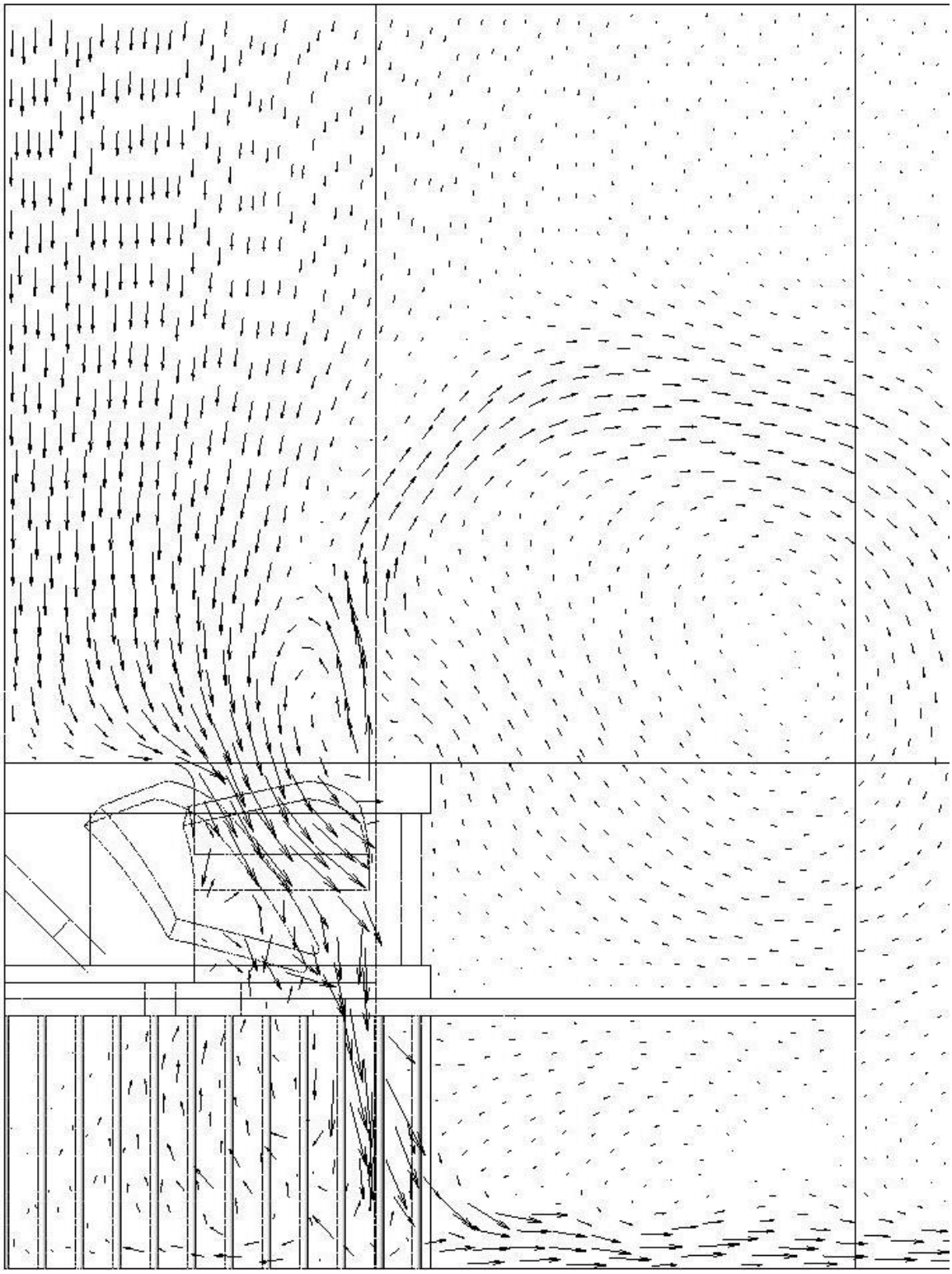

Figure 32: Velocity vector field of Case (4) on PLANE 1.

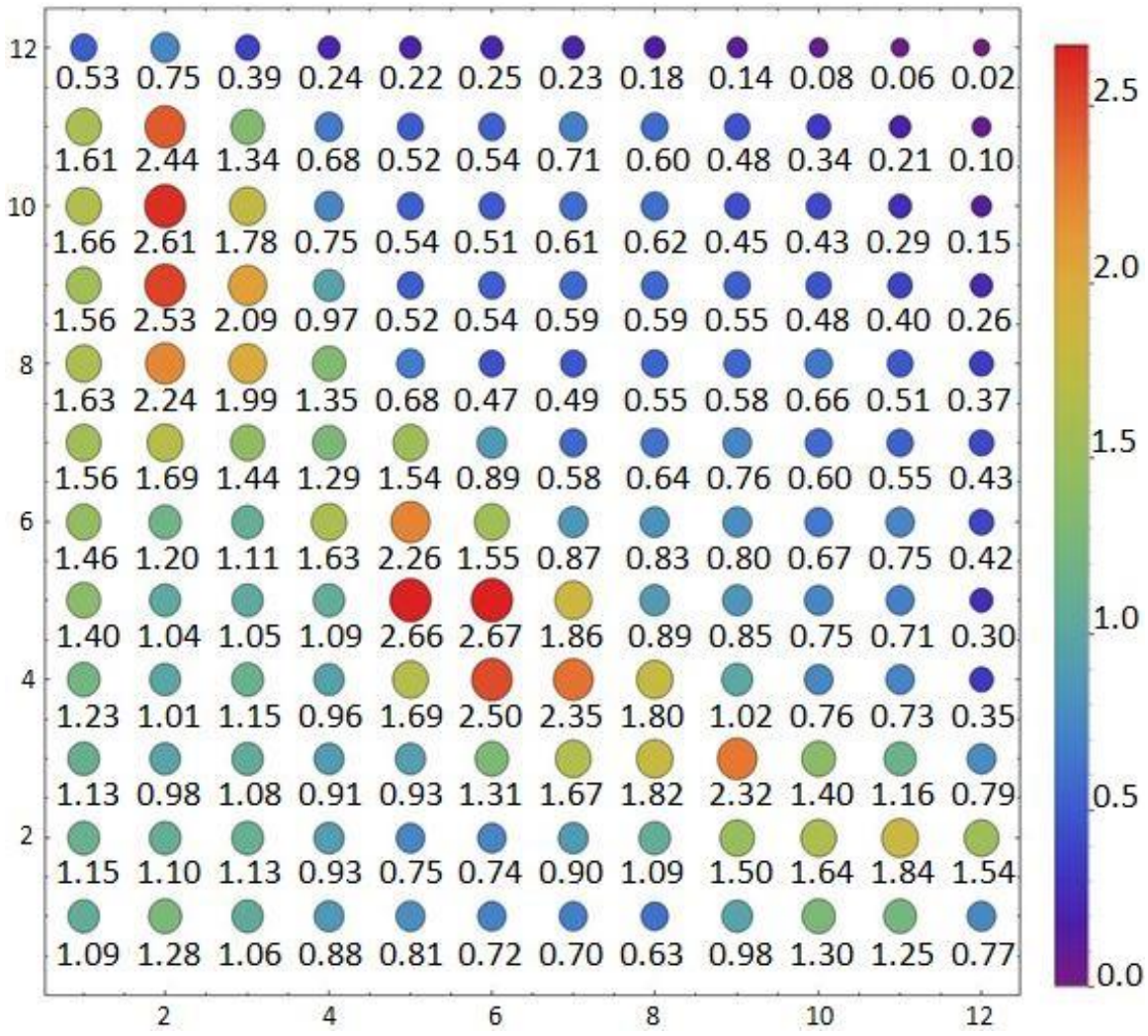

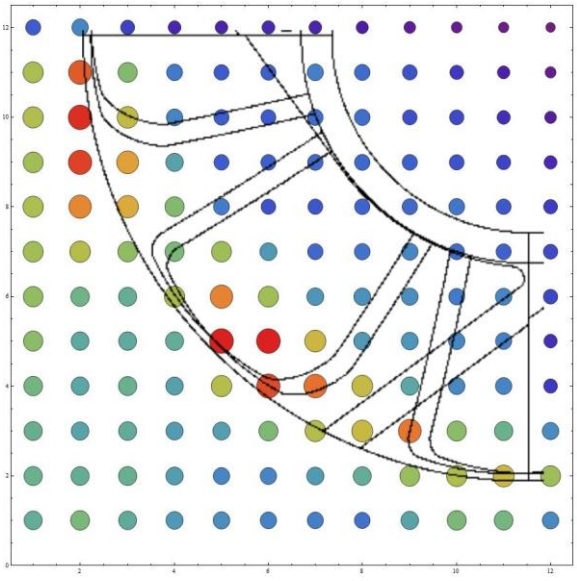

Figure 33: Rate of heat transfer of a given pin fin divided by the time averaged rate of heat transfer of the average fin for Case (4). This ratio is a dimensionless quantity indicating the effectiveness of a given fin at dissipating thermal energy. See text for a detailed description.
(a). The top image is a numerical representation of the ratio.
(b). The bottom image displays the location of the fan, hub, and housing.

the best heat transfer was found in the center, second best in the upper left, and third in the lower right. This asymmetry was due to airflow being blocked by the piece of housing shown in Figure 33(b). The reason the upper and center regions have equally good heat transfer in this case is due to slightly more airflow over the fins in line with the tips of the fan blades. This is evident from axial velocity contours, similar to those seen in Figures 13-16.

A temperature contour of Case (4) is shown in Figure 34, which displays data on PLANE 2. Due to the flow field being nearly the same as Case (1), the temperature contour is very similar as well. The coolest regions remain beneath the tips of the fan blades and the hottest regions beneath the fan hub and housing. The overall temperature appears slightly higher in the pin fin array in Figure 34 than Figure 19, but this is not in general true. Remember that this problem is transient, so parameters will fluctuate. The overall rate of heat transfer of the pin fins is just over 99% of Case (1), as seen in Table 4. This indicates that the shroud essentially did not affect heat transfer in this case. The original motivation for a shroud was to prevent the hot air leaving the pin fin array from traveling around the outside of the fan and recirculating back into the inlet of the fan. This has been seen to happen in a large amount of applications. Though not simulated, if a shroud had been used with Case (3), it is suspected the heat transfer would have increased as the hot fluid that recirculated around the housing of the fan would have been stopped. The author suggests the use of a shroud if it is known that the particular heat sink assembly induces recirculation.

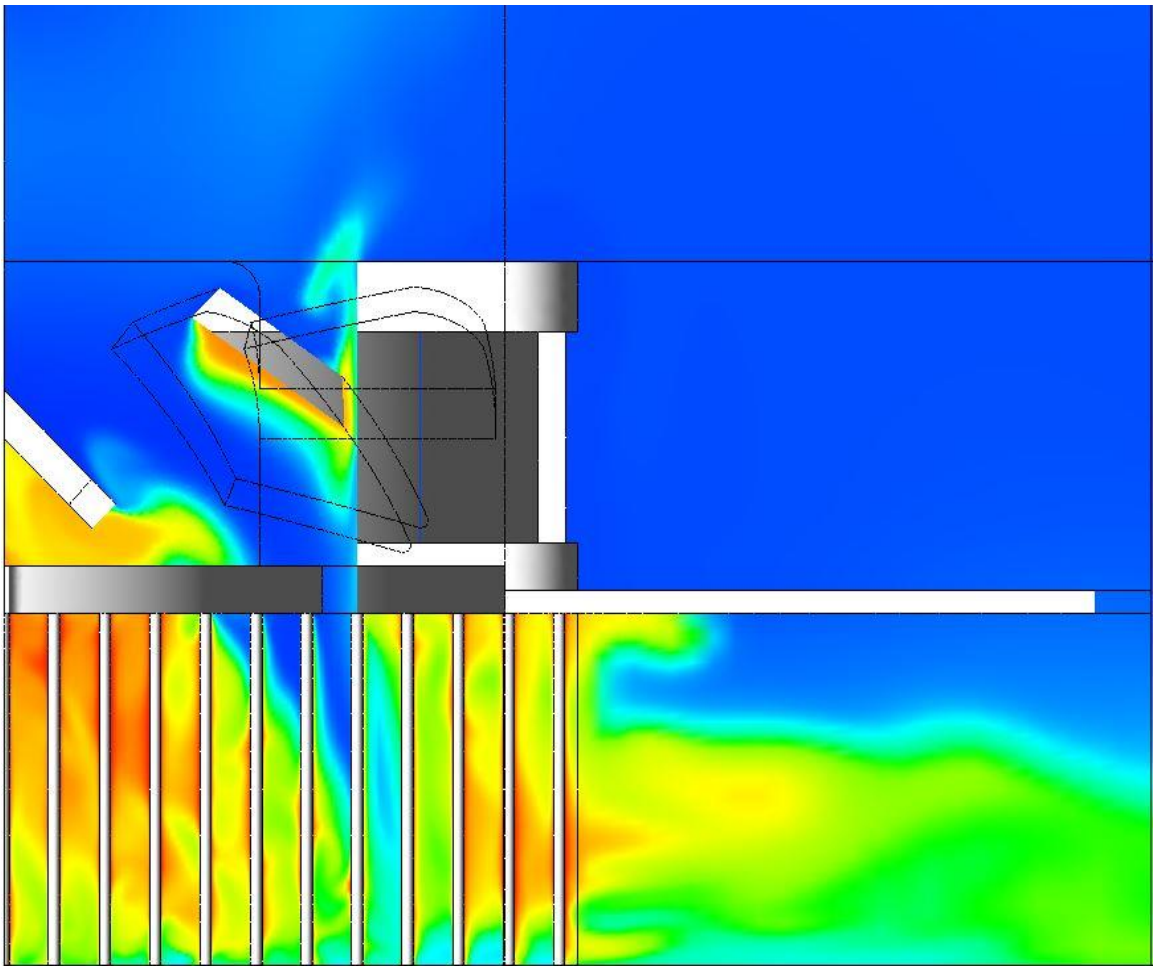

Figure 34: Temperature contour of Case (4) on PLANE 2.

Case (5)

Case (5) has the same parameters and geometry as Case (1), except the fan has been physically flipped, as to suck air off the fins rather than impinge onto them. A velocity vector field of Case (5) is presented in Figure 35. This figure is on PLANE1, as shown in Figure 10. It is clear from this figure that the system is not operating in the intended way. The motion of the air is very chaotic. Some air is entrained through the intended outlet of the fan, though not as much as seen in Case (1). Some of the activity within the pin fin

array is similar to Case (1), with high speeds at the tips of the fan blades and lower speeds underneath the fan hub and housing. Notably, the air is less stagnant beneath the fan hub in Case (5). A second velocity vector diagram of Case (5) on PLANE 2 is included to further contrast the two cases. Recall that a velocity vector diagram of Case (1) on PLANE 2 is in Figure 12. Notice the direction of the flow in the pin fin array has changed, as well as the overall magnitude is lower in Case (5). In sum, the fan is doing its best to move air in whichever way it can, though it is not doing so in a very well-directed way.

The dimensionless heat transfer ratio of each pin fin in Case (5) can be seen in Figure 37(a). General similarities, such as worst heat transfer beneath the fan hub and best heat transfer along the pin fins in line with the tips of the fan blades, are still true. However, the Case (5) is much more asymmetric due to the chaotic nature of the fluid flow. Seemingly random pin fins have good heat transfer while their neighbors have poor heat transfer. This is seen in row 12. When viewing velocity contours through these fins, it is indeed seen that the magnitude of the velocity is higher on these fins than their neighbors.

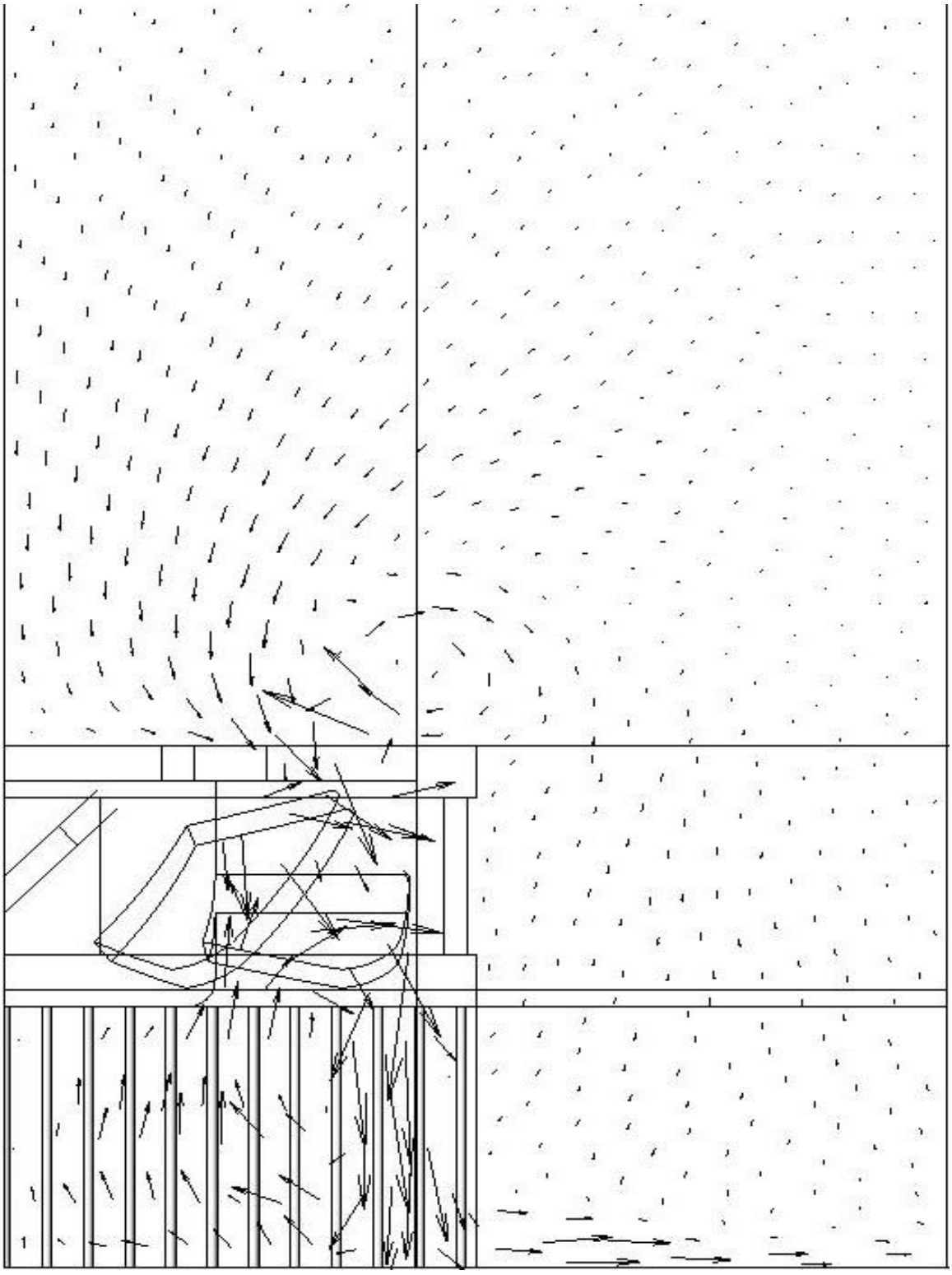

Figure 35: Velocity vector diagram of Case (5) on PLANE 1.

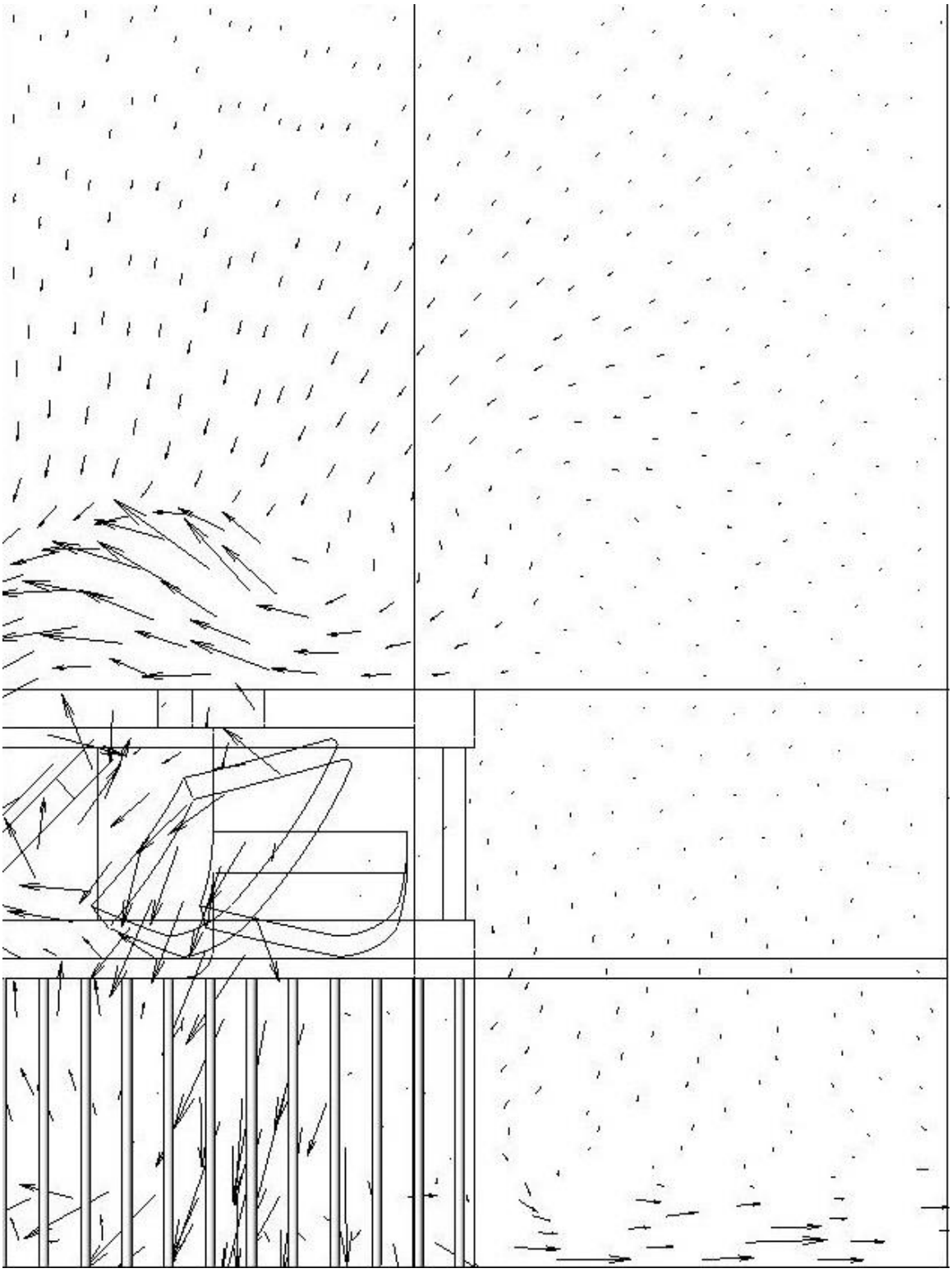

Figure 36: Velocity vector diagram of Case (5) on PLANE 2.

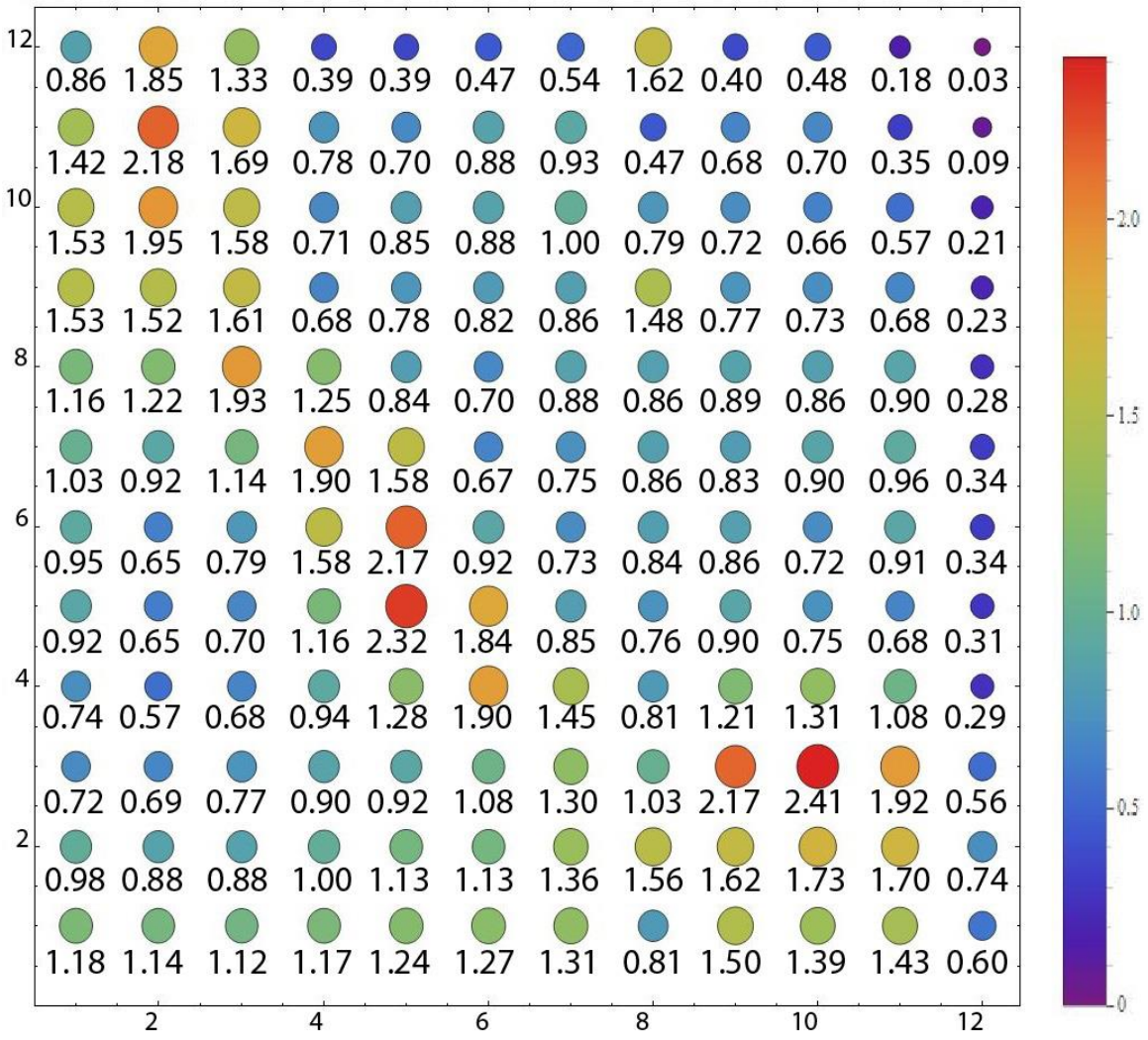

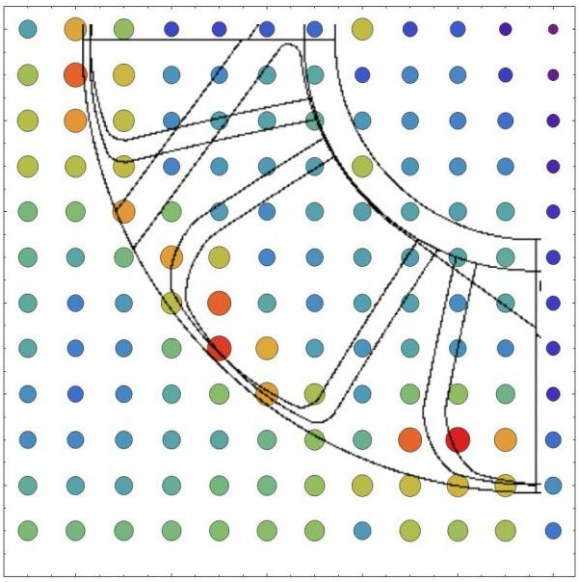

Figure 37: Rate of heat transfer of a given pin fin divided by the time averaged rate of heat transfer of the average fin for Case (5). This ratio is a dimensionless quantity indicating the effectiveness of a given fin at dissipating thermal energy. See text for a detailed description.
(a). The top image is a numerical representation of the ratio.
(b). The bottom image displays the location of the fan, hub, and housing.

A temperature contour of Case (5) on PLANE 1 is shown in Figure 38. The contour is similar to Case (1), seen in Figure 18, though there are notable differences. It is clear that the fan is unable to overcome the pressure drop caused by the pin fin array. The region at the intended outlet of the fan is hotter than in Case (1). The pin fin region below the fan hub is not has hot as in Case (1) due to the increased airflow which was seen the velocity vector fields. Temperatures are not as low at the base of the pin fin array, due to decreased airflow penetration. Heat is still primarily leaving with the air which exits along the base of the pin fin array. The overall heat transfer was around 92% of Case (1), indicating that it is better to have the fan impinge on the pin fin array than suck air off from it.

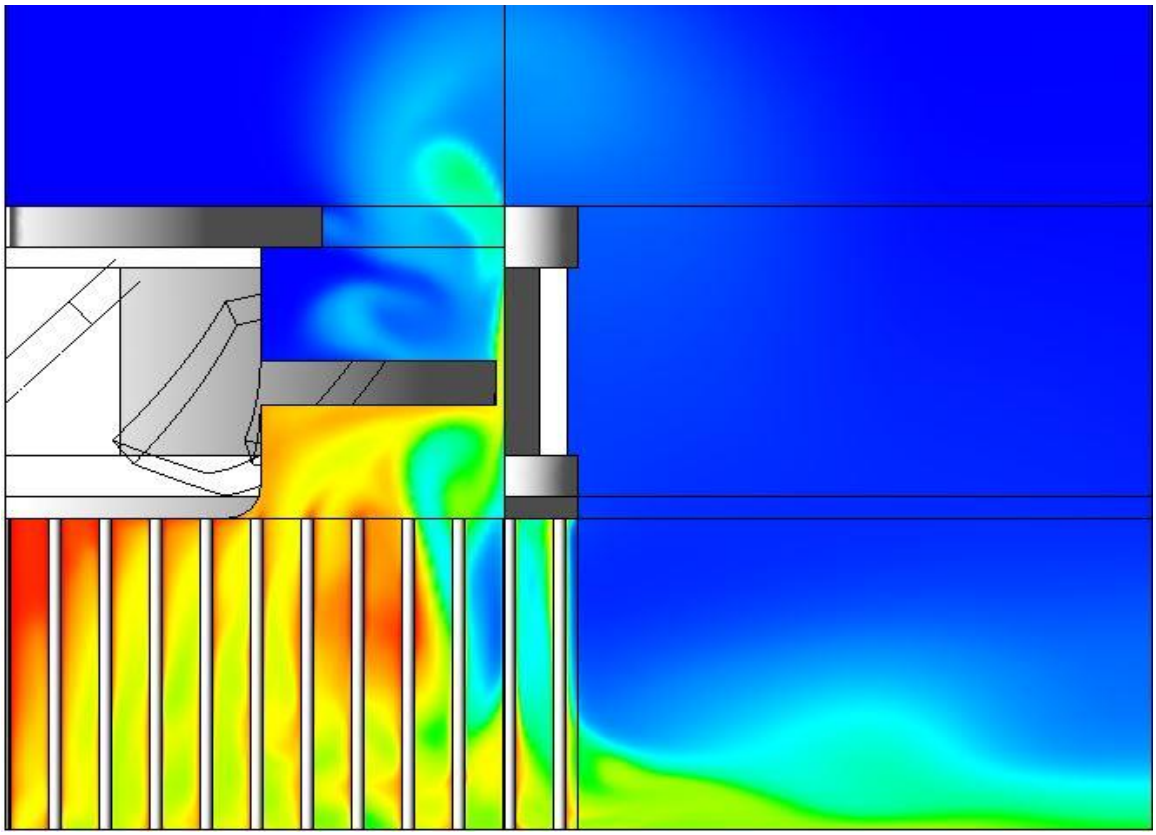

Figure 38: Temperature contour of Case (5) on PLANE 1.

Case Number	Overall Time Average Heat Transfer Rate (Watts)
Case (1): Baseline	1.12856
Case (2): Base temperature equal to one	1.06268
Case (3): 25 mm fins	1.42456
Case (4): Shrouded	1.12012
Case (5): Reversed Fan	1.04112

Table 4: Time averaged rate of heat transfer for the full pin fin array (not the quarter symmetry).

CONCLUDING REMARKS

Seemingly for the first time, the operation of a muffin fan used for the thermal management of electronic equipment has been modeled with high fidelity. In particular, the fan geometry and the rotation of its blades are properly accounted. The fan-provided airflow is of a highly complex nature. Not only is the flow unsteady, but it is also three-dimensional with a strong swirl component.

The electronic equipment considered here transfers its heat to an array of pin fins and, in turn, the fins are cooled by convectively by the coolant air that is provided by the muffin fan. The geometric structure of the muffin fan precludes the delivery of a uniform airflow to the pin-fin array. There are, in fact, structure-related blockages which significantly diminish the coolant flow arriving at fins which are situated downstream of the blockages. These "dead zones" diminish the overall efficiency of a thermal management system based on coolant air supplied by a muffin fan.

Numerical simulation served as the modeling and solution modality. The geometrical complexity limited the degree of parameterization. All told, five physical situations were considered, with one of these serving as a baseline. The primary results consisted of both per-fin local rates of heat transfer and array-total heat transfer rates. The patterns of fluid flow were exhibited by means of vector diagrams. Temperature and velocity distributions were displayed in color contour diagrams.

REFERENCES

[1] Agonafer, D., & Free, A. (1997). Conjugate Model of a Pin-Fin Heat Sink Using a Hybrid Conductance and CFD Model within an Integrated MCAE Tool. In Thermal Management of Electronic Systems II (pp. 53-62). Springer Netherlands.

[2] Behnia, M., Copeland, D., & Soodphakdee, D. (1998, May). A comparison of heat sink geometries for laminar forced convection: numerical simulation of periodically developed flow. In Thermal and Thermomechanical Phenomena in Electronic Systems, 1998. ITHERM'98. The Sixth Intersociety Conference on (pp. 310-315). IEEE.

[3] Maveety, J. G., & Jung, H. H. (2000). Design of an optimal pin-fin heat sink with air impingement cooling. *International Communications in Heat and Mass Transfer*, *27*(2), 229-240.

[4] Kobus, C. J., & Oshio, T. (2005). Development of a theoretical model for predicting the thermal performance characteristics of a vertical pin-fin array heat sink under combined forced and natural convection with impinging flow. International journal of heat and mass transfer, 48(6), 1053-1063.

[5] Shah, A., Sammakia, B. G., Srihari, H., & Ramakrishna, K. (2004). A numerical study of the thermal performance of an impingement heat sink-fin shape optimization. IEEE Transactions on Components and Packaging Technologies, 27(4), 710-717.

[6] Zheng, N., & Wirtz, R. A. (2002). Cylindrical pin-fin fan-sink heat transfer and pressure drop correlations. Components and Packaging Technologies, IEEE Transactions on, 25(1), 15-22.

[7] Jonsson, H., & Moshfegh, B. (2001). Modeling of the thermal and hydraulic performance of plate fin, strip fin, and pin fin heat sinks-influence of flow bypass. Components and Packaging Technologies, IEEE Transactions on, 24(2), 142-149.

[8] Park, K., Choi, D. H., & Lee, K. S. (2004). Numerical shape optimization for high performance of a heat sink with pin-fins. *Numerical Heat Transfer, Part A: Applications*, *46*(9), 909-927.

[9] Jian-Hui, Z., & Chun-Xin, Y. (2008). Design and simulation of the cpu fan and heat sinks. Components and Packaging Technologies, IEEE Transactions on, 31(4), 890-903.

[10] Huang, C. H., Lu, J. J., & Ay, H. (2011). A three-dimensional heat sink module design problem with experimental verification. International Journal of Heat and Mass Transfer, 54(7), 1482-1492.

[11] F. R. Menter, "Two-equation eddy-viscosity turbulence models for engineering applications," AIAA Journal, vol. 32, no. 8, pp. 1598–1605, 1994.

[12] B. E. Launder and D. B. Spalding, "The numerical computation of turbulent flows," Computer Methods in Applied Mechanics and Engineering, vol. 3, no. 2, pp. 269–289, 1974.

[13] D. C. Wilcox, “Reassessment of the scale-determining equation for advanced turbulence models,” AIAA Journal, vol. 26, no. 11, pp. 1299–1310, 1988.

[14] D. C. Wilcox, “Comparison of two-equation turbulence models for boundary layers with pressure gradient,” AIAA journal, vol. 31, no. 8, pp. 1414–1421, 1993.